NATIONAL AERONAUTICS AND SPACE ADMINISTRATION

Technical Memorandum 33-780

An Experimental Investigation of Fluid Flow and Heating in Various Resonance Tube Modes

JET PROPULSION LABORATORY
CALIFORNIA INSTITUTE OF TECHNOLOGY
PASADENA, CALIFORNIA

September 1, 1976

PREFACE

The work described in this report was performed by the Propulsion Division of the Jet Propulsion Laboratory.

ACKNOWLEDGEMENT

The authors are grateful to Paul F. Massier for valuable guidance in this research and to Wayne Bixler, Scotty Slover, Stanley Kikkert, and Don Feller for technical assistance in conducting the experiments.

CONTENTS

CONTENTS (contd)

FIGURES

FIGURES

ABSTRACT

Experiments have been performed to study resonance phenomena in tubes excited by underexpanded jet flows. This investigation comprised the following: study of the various resonance tube modes under a wide range of nozzle pressure, spacing between nozzle and tube mouth, and different tube length; the effects of these modes on the endwall pressure and gas temperature; flow visualization of both jet and tube flows by spark shadowgraph technique; and measurement of wave speed inside the tube by the laser-Schlieren techniques. An extensive study of the free-jet flow was undertaken to explain important aspects of various modes of operation of resonance tube flows.

I. SUMMARY

An experimental investigation has been conducted to determine the basic mechanism of heating in constant cross-sectional resonance tubes excited by underexpanded jet flows. The jet flow between the nozzle exit and the tube inlet plays a key role in the performance of a resonance tube. A detailed and systematic investigation of the unsteady complex shock structure in this part of the flow region has led to a better understanding of the fundamental mechanisms associated with the gas heating in such tubes. A study of the effects of tube location in relation to free-jet shock location (without the presence of the resonance tube) has shed further light on the underlying mechanism of sustained oscillations of the flow in a resonance tube.

To understand the basic features of resonance tube flows, a system was constructed consisting of a nitrogen jet at room stagnation temperature, discharging from a convergent nozzle of 2.03-cm exit diameter into the resonance tube. Most of the resonance tubes were square in cross section with a width of 2.54 cm and with lengths of 7.6, 17.8, and 35.6 cm. The square tubes had transparent sidewalls made of lucite. Experiments were also performed using a round stainless steel tube which had a diameter of 2.54 cm and a length of 35.6 cm. The effects of nozzle pressure ratios R (up to 8.2 atmospheres) and the tube spacings s/d (1 to 4) on the endwall gas temperature were studied for various tube lengths. The resonance tube flows were studied over a wide range of nozzle pressures and tube spacing by taking endwall pressure traces and analyzing the still and motion pictures taken by spark shadowgraph technique. Measurements of the wave speed inside the tube were made by using a laser-Schlieren technique and simultaneously studying the output of two pressure transducers installed flush with the sidewall, a known distance apart.

The present study indicated that resonance tube flows can operate in three modes, depending upon nozzle pressure ratio, tube-nozzle spacing and tube geometry. The three modes are defined as (1) jet instability mode, (2) jet regurgitant mode, and (3) jet screech mode.

The jet instability mode occurred only for subsonic jet flows. Spark shadowgraphs showed the formation of toroidal vortices in the jet flow. These toroidal vortices grew in size as they convected downstream towards the tube inlet and resulted in weak compression waves inside the tube. The oscillation frequency of the jet flow in this mode was found to occur in a band of nondimensional frequency $fd/U_j \approx 0.3$ to 0.4. The weak shock waves formed in this mode of operation did not produce any significant increase in the gas temperature measured at the endwall.

In the jet regurgitant mode of operation, which occurred for both subsonic and supersonic jets, periodic swallowing of the nozzle jet and its efflux from the resonance tube occurred at the fundamental resonance frequency of the tube. This is given by $f \approx a/4L$, where f is the frequency of jet swallowing, the quantity a is the average speed of sound inside the tube, and L is the tube length. In this mode of operation, most of the gas heating resulted from the dissipative heat generated by the formation of shock waves inside the tube. Wave speeds inside the resonance tube in the jet regurgitant mode of operation agreed well with simple shock reflection theory from the tube endwall. In this mode, pressures below atmospheric pressure were observed at the tube endwall before the beginning of the inflow phase. Behind the incident shock wave, pressures were close to atmospheric pressure, as proposed by Brocher et al. (Ref. 1).

The resonance tube flow system switched to the jet screech mode when the tube spacing was equal to the free-jet shock location, i.e.,

$$\frac{s}{d} \approx \left(\frac{X_s}{d}\right)_{\text{free-jet}}$$

This mode occurred when the jet flow was supersonic. In the jet screech mode, a normal shock constantly stood between the nozzle exit and the tube entrance and oscillated at high frequency.

The present study showed that large turbulent mixing between the cold nozzle-jet flow and the oscillating hot tube flow occurred in the inflow phase of the jet regurgitant mode. Most of the heat generated by shock wave dissipation in the tube was carried away by the tube jet in the outflow phase.

This outflow seems to be the dominant source of heat removal from resonance tubes and consequently is the most significant factor in limiting the endwall gas temperature in the jet regurgitant mode. In the jet screech mode of operation, these losses were minimal. If the resonance tube is tuned to the frequency of the screeching shock wave oscillation (formed in the jet flow between the nozzle exit and the tube inlet), intense and rapid heating of the trapped tube gas results. The highest endwall gas temperature was about 900 K before tube failure occurred because of overheating the lucite walls.

This investigation also showed that any leaks which existed in resonance tubes had a devastating effect on the heating of the gas. High gas temperatures simply could not be obtained when leaks occurred in the vicinity of the endwall or through the interface between the sidewalls.

II. INTRODUCTION

Since Hartmann's discovery of the resonance tube phenomenon in 1919 (Ref. 2), many researchers have investigated certain aspects of the fluid dynamics associated with this device. It has long been known that for a wide range of resonance tube configurations such as length of the tube, spacing between the nozzle exit and the tube inlet, nozzle-to-tube-diameter ratio, length of the tube, and nozzle flow conditions, intense and very rapid heating of the gas near the endwall can be obtained. This can occur when either subsonic or supersonic jet flows impinge on the open end of the tube. The characteristics of the rapid intense heating of the endwall tube gas have led investigators to consider the application of resonance tubes as a possible method of igniting a rocket engine (Refs. 3 and 4) or as an escape system for an air crew from an aircraft (Ref. 5). Resonance tube flows are also of interest because the intense heating of the tube gas is accompanied by generation of high-intensity ultrasonic waves (Ref. 6) which can be employed for ultrasonic drying and for fog dissipation (Ref. 7).

According to Hartmann (Ref. 2), high-intensity sound waves are generated when an air-jet oscillator such as the resonance tube is placed in the region where the pressure in the jet is rising, i. e., the so-called "zones of

instability." This high-intensity ultrasonic sound generation by the air-jet generator when placed in these zones of jet instabilities showed a large amplitude of almost normal shock wave oscillation in front of the air-jet generator inlet (cf. Plate IX, Ref. 2). The frequency of this shock wave oscillation in the "zone of instability" decreases with increasing distance between the nozzle exit and the inlet of the air-jet generator. These large-amplitude oscillations of the shock wave in the jet-flow disappear and reappear with varying spacing between the nozzle exit and the tube inlet. However, no detailed and systematic investigation of this mode of air-jet generator on heating of the tube gas has been undertaken.

Sprenger (Ref. 8) studied at length the effects that nozzle-tube spacing, nozzle stagnation pressure, and length of the tube have on the endwall tube temperature. For a given resonance tube and jet flow, many peaks in the endwall tube temperature about as high as 750 K were observed. It was also noticed that for a given resonance tube, large variations in endwall gas temperature were noticed when slight changes in nozzle pressure ratio or spacing between the nozzle exit and the tube inlet were made. However, no detailed study was undertaken to investigate the resonance tube flows that produced the drastic changes in the endwall temperature.

Previous work on the fluid dynamics of resonance tubes has been mainly experimental. Most of the investigators in the past (Refs. 1, 8-12) concentrated on the particular mode of resonance tube operation in which the jet flow between the nozzle exit and tube inlet is periodically swallowed by the tube. As compared to Hartmann's resonance tube operation with tube inlet located in the spatial zones of instability, in this periodic jet swallowing mode of operation, quite unique periodic shock wave structure in the jet flow results (Ref. 9). Under certain conditions of flow and tube configuration, in this periodic swallowing mode of resonance tube operation, shock waves are formed inside the tube (Refs. 1, 9, 11 and 12). The frequency of shock wave oscillations in the tube is at the tube fundamental frequency given by $f \approx a/4L$. Most of the heating in the tube is caused by the dissipation processes, i. e., increase in the entropy, through the shock waves (Ref. 1).

Many attempts have been made to predict the maximum attainable gas temperatures in resonance tubes in the jet regurgitant mode of operation

(Refs. 13 and 14). The predicted temperatures in these investigations are very high compared to the measured temperatures. It is felt that the detailed study of the tube flow in this mode of operation will shed more light on the various heat loss mechanisms (other than wall conduction which is thought to be the main source of heat loss from the tube) which limit the attainable temperatures in the tube. It is strongly felt that a detailed investigation of wave speed and flow inside the tube during various phases of jet regurgitant mode cycle is needed. These experimental observations along with pressure and temperature measurements in this mode of operation will be of great assistance in predicting the resonance tube performance accurately.

Although there is a fair amount of knowledge about the regurgitant mode of the resonance tube, little is known about the thermal effects for the mode of operation in which a normal shock wave stands in the resonance tube jet flow and oscillates at high frequency (Refs. 2, 7 and 15). Frequency of shock oscillation in the jet flow in this mode of operation strongly depends upon shock spacing s/d, pressure ratio R, etc., and is virtually independent of the length of the resonance tube (Refs. 2 and 4).

In the present study, the effects of nozzle flow and of tube configuration on tube gas heating for various resonance tube modes of operation were investigated. The jet flow between the nozzle exit and tube inlet plays a key role in the resonance tube performance. An investigation of the unsteady complex shock structure in this part of the resonance tube flow has led to a better understanding of the fundamental mechanism associated with gas heating in such tubes. The structure of the jet flow located between the nozzle exit and tube inlet was correlated with the free-jet structure, i.e., without the presence of the tube. Of particular interest is the mode of operation in which rapid intense heating of the tube gas occurs.

III. EXPERIMENTAL APPARATUS, INSTRUMENTATION, AND TEST PROCEDURES

A. RESONANCE TUBE CONFIGURATIONS AND NOZZLE FLOW CONDITIONS

The various modes of resonance tube operation were investigated using the apparatus shown in Figs. 1 and 2. Most of the tubes were square in cross section, having a width of 2.54 cm. With the square tubes, data were obtained for three different tube lengths: 7.6, 17.8, and 35.6 cm. Experiments were also conducted using a round stainless steel tube which had a diameter of 2.54 cm and a length of 35.6 cm.

The side walls of the square tubes were lucite so that wave speeds could be determined and the tube flow could be visualized. The endwall and the upper and lower tube walls were made of micarta. For any given test, the centerline of the nozzle was aligned with that of the tube inlet. In Fig. 1, the tube inlet was located behind the deflector shield and is not visible. Compressed nitrogen at ambient stagnation temperature was expanded through the convergent nozzle, which had an exit diameter $d = 2.03$ cm. The ratio of the width of the square cross-sectional tube or the diameter of the steel resonance tube-to-nozzle exit diameter $D/d = 1.25$ was kept constant throughout these experiments. The nozzle pressure ratio R, could be varied up to a value of approximately 8.2. The spacing between the tube entrance and the nozzle exit was adjusted at values of $s/d = 1.0$, 1.5, 1.75, 2.0, 3.0, 3.5, and 4.0. A deflector shield which had an outer diameter of 33 cm was placed at the entrance of the resonance tube (see Fig. 1). It prevented the nitrogen from flowing over the outside of the tube. This allowed flow visualization as well as wave speed measurements inside the tube without the disturbances from the flow around the tube. The flow conditions at which the resonance tubes were tested are given in Table 1.

B. MEASUREMENTS

Both endwall temperature and endwall pressure traces as a function of time were obtained at different nozzle pressure ratios and various spacings between the tube inlet and the nozzle exit and for different tube lengths. The gas temperature was measured with 40-gage chromel-alumel wire of

Table 1. Resonance tubes tested and conditions

Sonic nozzle contraction area ratio = 4

Resonance tube to nozzle exit diameter ratio, D/d = 1.25

Driver gas, nitrogen (total temperature, 290 K)

Conditions	Square cross section	Circular cross section
Nozzle total pressure range	10.13 to 83.09 N/cm^2 (1.0 to 8.2 atm)	10.13 to 56.74 N/cm^2 (1.0 to 5.6 atm)
Sidewall material	Upper/lower: Micarta sides: Lucite	321 stainless steel
Sidewall thickness	All 4 walls, 1.27 cm	0.025 cm
Endwall material	Micarta	321 stainless steel
Nozzle to tube spacing, s/d	1.0 to 6.0	1.0 to 6.0
Tube length, cm (L/D)	7.6 (3), 17.8 (7) and 35.6 (14)	35.6 (14)
Remarks	Wave speed measurements inside the tube by laser-Schlieren technique. Spark shadowgraph pictures taken of jet and tube flow	Nine thermocouples installed to outer wall at locations from endwall of x/D = 0.25, and increments of 1.5D thereafter. Spark shadowgraph pictures taken of jet flow

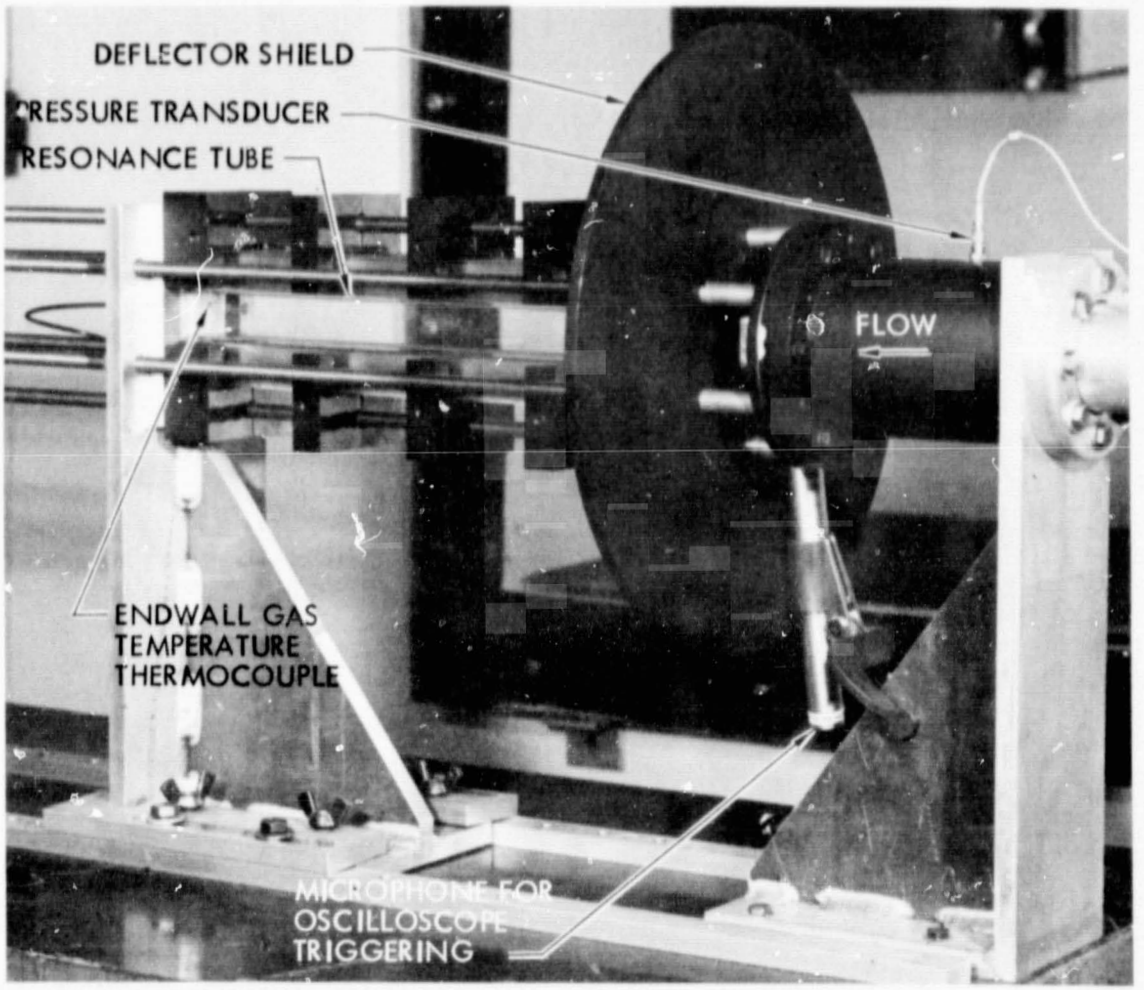

Fig. 1. Resonance tube system

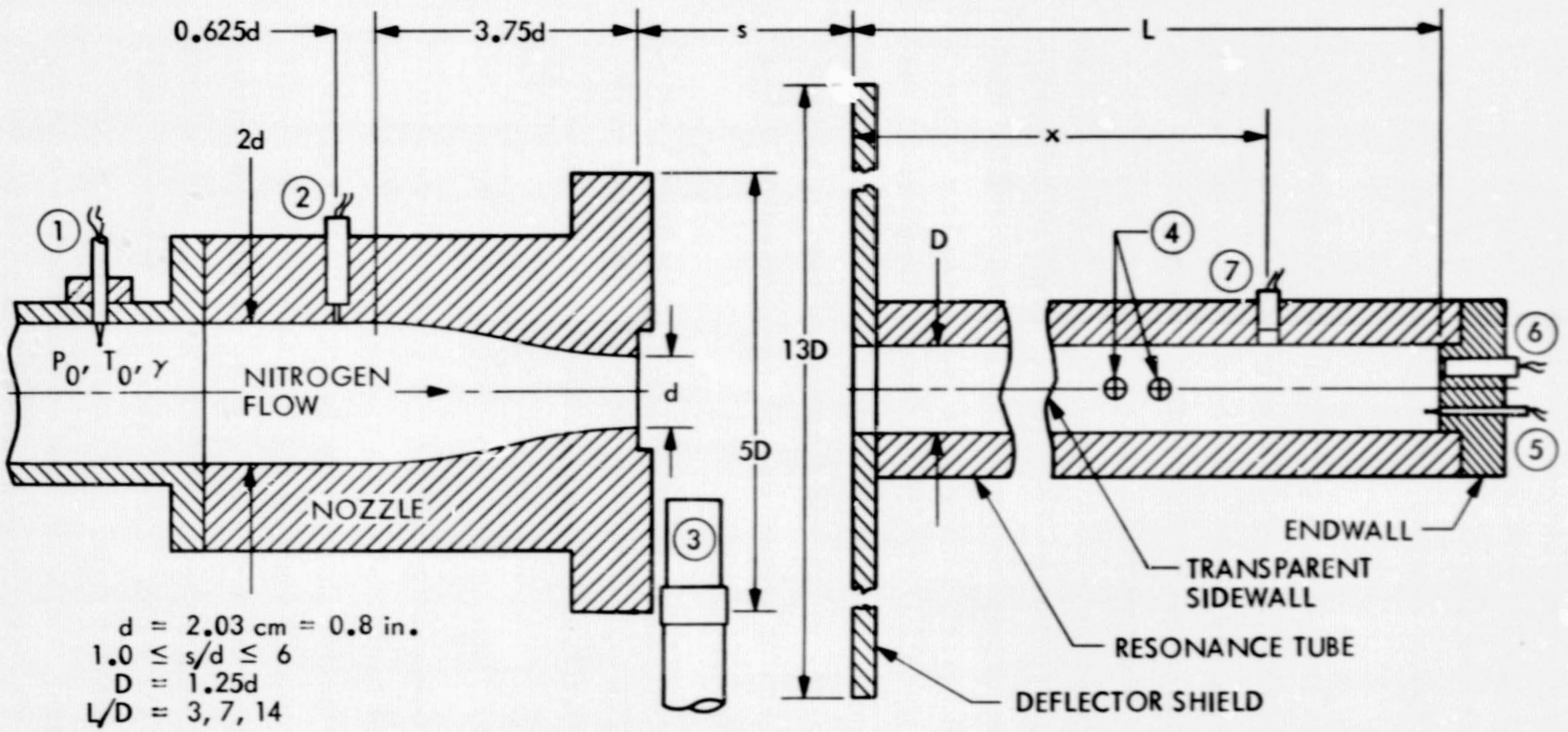

(1) TOTAL TEMPERATURE THERMOCOUPLE (22 GAGE CHROMEL-ALUMEL WIRE)

(2) PRESSURE TRANSDUCER (KISTLER MODEL 601A)

(3) MICROPHONE TRIGGER FOR OSCILLOSCOPE RECORDING

(4) LASER BEAM PAIR FOR WAVE VELOCITY MEASUREMENT (VARIABLE SPACING AND VARIABLE AXIAL LOCATION)

(5) ENDWALL GAS-TEMPERATURE THERMOCOUPLE (40 GAGE CHROMEL-ALUMEL WIRE)

(6) ENDWALL PRESSURE TRANSDUCER (KISTLER MODEL 208)

(7) SIDEWALL PRESSURE TRANSDUCER (KISTLER MODELS 601A AND 208 AT x/D = 6, 12)

Fig. 2. Resonance tube apparatus and instrumentation

0.007-cm (0.003-in. diameter). The response time of these thermocouples in the present experiments was estimated to be approximately 50 millisec or less. Similar thermocouples were installed on the outside of the stainless steel tube. The output of these thermocouples was recorded on an oscilloscope. A microphone located close to the jet flow (Fig. 2) was used to trigger the oscilloscope.

Kistler pressure transducers (Models 208 and 601A) flush-mounted on the endwall were used to obtain fluctuating pressure inside the tube. These transducers had a resolution of 0.014 N/cm^2 (0.02 psi) with a rise time of 2 μsec. The frequency response of the pressure transducers was from 2 to 40,000 Hz. The output of the transducers drifted as the temperature increased; therefore, these transducers could only be used for determining the pressure jumps in a trace. To determine absolute levels of the pressures inside the tube in a cycle, pressure transducers were installed flush with the sidewall. The absolute levels of pressure inside the resonance tube were indirectly determined by studying the pressure jump across the incident and reflected shock waves close to the endwall. In addition, it was necessary to know the wave speed, which was determined both by a laser - Schlieren technique and by observing simultaneously the pressures at two locations a known distance apart on the sidewall.

During the course of this study, it was found that leaks have a severe effect on tube performance. Therefore, before any measurements were obtained, the tubes were pressurized to 30 psig and checked for leaks.

C. OPTICAL INSTRUMENTATION

The laser-Schlieren technique employed to measure wave velocity inside the square tubes utilized two parallel laser beams, spaced a known distance apart, which were projected through the lucite walls and sensed by two photomultipliers. The beams were partially intercepted by a knife edge before they reached the photomultipliers. As the wave passed across one laser beam, the emerging beam was deflected by an angle proportional to the density gradient across the wave. A Schlieren system was set up by intercepting this part of the deflected light. By cross-correlating data from the two beams, the incident, reflected, and contact surface velocities in the tube were determined. The beams were moved along the length of

the tube to measure the velocities at different axial locations along the tube.

Instant spark shadowgraphs as well as motion pictures of the resonance tube flows were taken using an electronic strobotac. The flash duration of this strobotac was less than 3 μsec, during which time the resonance tube flow was photographed. This duration was short enough to "freeze" the flow field.

Instant shock structure of a free-jet flow without the tube installed as well as of the flow with the resonance tube in place was obtained at various nozzle pressure ratios R and for different resonance tube configurations. By adjusting the flashing rate of the strobotac to an integral multiple of the speed of the jet shock-wave oscillation frequency, a stationary shock structure was observed. The flashing rate could be varied between 110 and 25,000 flashes/min. Also, by flashing near to but not synchronized with the shock-wave oscillation frequency, a slow-motion replica of the actual motion was observed. This information was used to arrange the random still shadowgraphs of the jet flow between the nozzle exit and the tube inlet in a sequence appropriate to events within a cycle of tube operation.

IV. EXPERIMENTAL RESULTS

A. VARIOUS MODES OF RESONANCE TUBE OPERATION

On the basis of a detailed and systematic investigation over a wide range of nozzle pressure ratios R, spacing ratios s/d, and resonance tube lengths L, the resonance tube flows can be divided into three modes of operation. These are defined as

(1) Jet instability mode.

(2) Jet regurgitant mode.

(3) Jet screech mode.

A description of each of these modes, the conditions under which they occur, and the physical processes involved will be discussed in the following sections.

1. Jet Instability Mode

This mode of resonance tube operation occurred only for a subsonic jet, i.e., $R < 1.9$ over a wide range of spacing s/d. Spark shadowgraphs of the jet flow, as will be discussed later, indicated the formation of large periodic vortices at the nozzle exit. These toroidal vortices in the jet flow grew in size as they convected downstream and resulted in weak compression waves inside the tube. These waves had a frequency equal to that of the vortex shedding frequency. The oscillation frequency of the jet flow in this mode was found to occur in a narrow range of nondimensional frequency parameter $fd/U_j \simeq 0.3$ to 0.4. For certain flow conditions and tube configurations, this oscillation frequency was superimposed on the fundamental tube resonance frequency $f \simeq a/4L$. The weak shock waves formed in the resonance tube in this mode of operation did not result in any significant increase in the gas temperature measured at the endwall. As the nozzle pressure ratio R was increased above 1.9, a periodic shock structure appeared in the jet flow between nozzle exit and the tube inlet. Depending upon the spacing s/d, the tube flow switched either to the regurgitant mode or to the screech mode of operation. These two modes are discussed in the next two sections.

2. Jet Regurgitant Mode

The jet regurgitant mode, as has been observed by other investigators (Refs. 1, 8 - 12), consists of periodic swallowing and discharging of the jet flow by the tube at the fundamental tube resonance frequency $f \simeq a/4L$. From the present spark shadowgraph pictures and from endwall pressure and temperature measurements, it has been concluded that:

(1) The first part of the regurgitant mode of tube operation was the inflow phase of the tube. Most of the jet flow entered the tube. Depending on the nozzle pressure ratio R, either a diamond cell shock structure or a barrel shock was present in front of the inlet of the tube. The jet shock wave structure in this phase of the cycle depended only on the initial condition: nozzle diameter, nozzle pressure ratio R, etc. That is, the jet flow between the nozzle exit and tube inlet behaved as if the tube was not present in the jet flow. The portion of the jet flow that entered the tube caused

the formation of compression waves. These compression waves then travelled toward the endwall. Coalescence of the compression wave train to a shock wave depended on tube length. In one case an almost normal shock wave was formed or else there was a shock wave which was followed by a train of compression waves. These waves were reflected as a shock wave or a shock wave followed by a train of compression waves. The strengthening of the shock wave by coalescence of compression waves continued until this reflected wave front reached the inlet of the tube. From there the compression wave front resulted in the formation of a strong expansion wave front which travelled into the tube. The flow then suddenly switched to a transition phase followed by the outflow phase of its cycle in the regurgitant mode.

(2) The presence of the expansion waves and reduced pressure behind the wave front caused the gas in the tube to flow outwards. The transition from inflow to the outflow phase resulted in a collision of the nozzle-jet and the tube-jet flows, thereby forming an interface. As the tube-jet flow gained in strength, the plane of the interface moved toward the nozzle.

(3) At the end of the transition period between the inflow and the outflow phases, the two opposing jet flows remained in this stage almost the same length of time as the inflow phase of the jet regurgitant mode. The outflow phase of the tube was completed as the expansion fan approached the tube inlet after reflection from the end wall. This resulted in a sudden weakening of the tube-jet flow.

(4) As the tube flow weakened, the interface quickly moved toward the inlet of the tube. Then the nozzle flow again reverted back to the inflow phase of the regurgitant mode of resonance tube operation, and thus one cycle of operation was completed at the tube fundamental frequency $f \simeq a/4L$. As compared to transition from tube inflow to outflow, the time required in switching from the outflow phase to the inflow phase was relatively short.

The actual duration of the various phases of a typical resonance tube cycle was not measured. Thompson (Ref. 9) studied at length the time required to complete these phases of a cycle of jet regurgitant mode. Similar conclusions as drawn above were reached. The structure of the flow inside the tube during the regurgitant mode of resonance tube operation will be discussed in Section IIIB.

3. Jet Screech Mode

As previously discussed, in the inflow phase of the jet regurgitant mode, the jet flow between the nozzle exit and the tube inlet behaved like a free jet, i.e., without the presence of the tube in the jet flow. The jet flow went through this part of the regurgitant mode cycle if the spacing s/d was greater than the free-jet shock location $(X_s/d)_{free\text{-}jet}$. But as the pressure was increased for a given tube spacing, $(X_s/d)_{free\text{-}jet}$ increased, until a nozzle pressure ratio R was reached for which $s/d = (X_s/d)_{free\text{-}jet}$. The present experiments indicated that the jet flow between the nozzle exit and the tube mouth then switched suddenly from the jet regurgitant mode and resulted in the formation of an almost normal shock in front of the inlet of the resonance tube. This shock oscillated at high frequency. Presence of this oscillating, almost normal shock wave (frequency as high as 20 kHz in this study) in front of the resonance tube inlet has led us to call this the jet screech mode of resonance tube operation. The strength and location of this shock as well as its oscillation frequency depended upon the spacing s/d, nozzle pressure ratio P., and the resonance tube inlet configuration. This mode of resonance tube operation is defined as the jet screech mode. Therefore, the boundary between the screech and regurgitant modes of operation is given by $s/d = (X_s/d)_{free\text{-}jet}$; i.e., the spacing is equal to the location of the shock in the free-jet. For $(X_s/d)_{free\text{-}jet} \gtrsim s/d$, the resonance tube operated in the screech mode and the jet flow was prevented from going into the filling phase of the tube (in the steady inflow phase as discussed previously under the jet regurgitant mode).

The experimental results that support these conclusions are shown in Fig. 3. This figure indicates the results of shock location X_s/d, in the jet flow between the nozzle exit and the tube inlet for the 35.6-cm resonance tube with spacing s/d = 1.5 and 3.0 at different nozzle pressure ratios R.

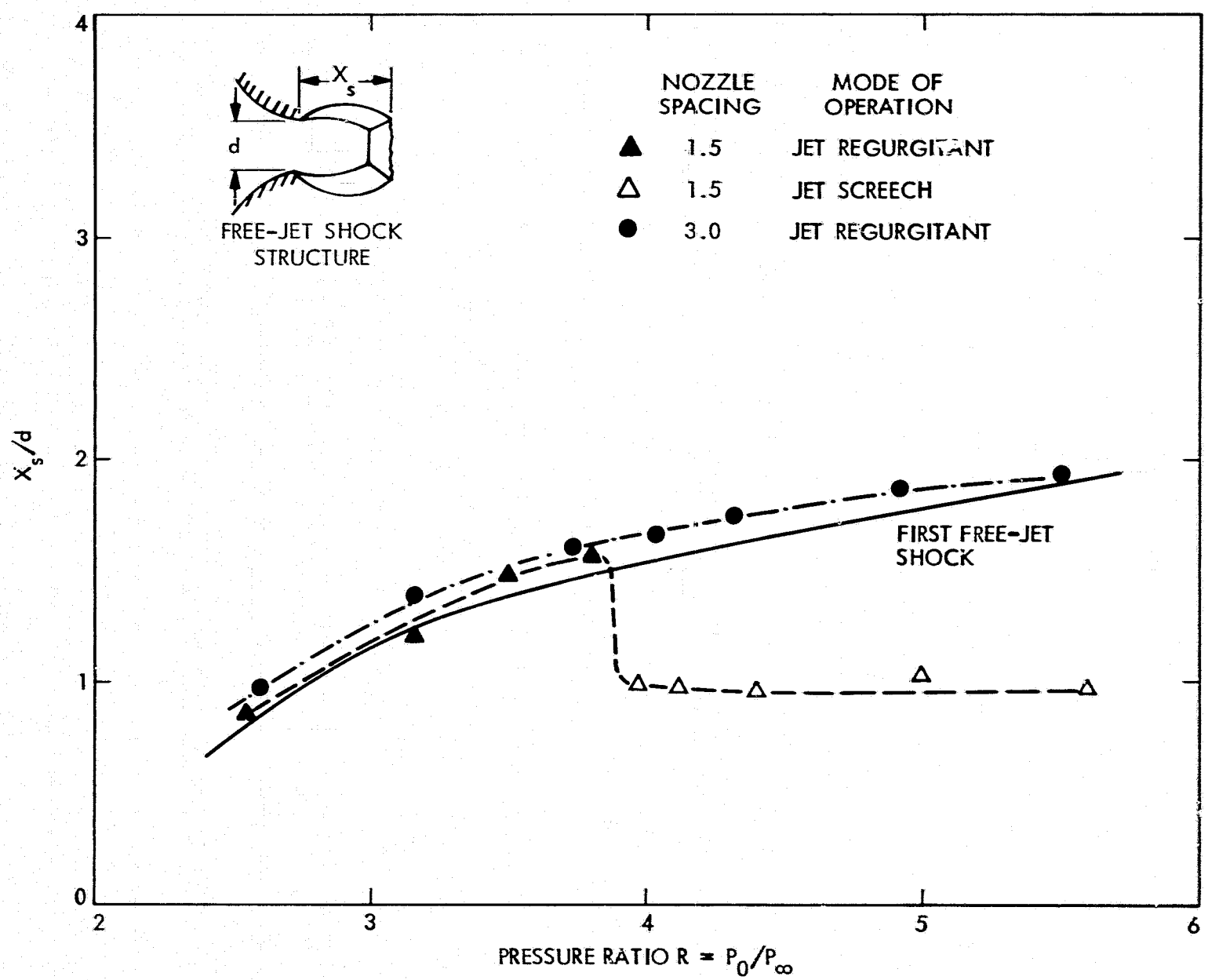

Fig. 3. Effect of nozzle pressure ratio R on shock wave location during 35.6-cm tube jet-filling phase in regurgitant and screech modes of operation

The location of the free-jet shock, $(X_s/d)_{free\text{-}jet}$ as a function of R is also indicated. The experimental points in the regurgitant mode in Fig. 3 show the position of the shock X_s/d, in the filling or inflow phase. For the jet screech mode, Fig. 3 indicates the mean position of the oscillating normal shock in front of the inlet of the resonance tube.

As expected, up to a spacing $s/d = 1.5$, the experimental points for the shock location X_s/d, in the inflow phase of the regurgitant mode lie on the free-jet shock location $(X_s/d)_{free\text{-}jet}$. Therefore, the jet flow in the filling phase of the jet regurgitant mode of operation behaves as if the tube were not present in the flow. This behavior of the jet continued until a pressure ratio $P_o/P_\infty = 3.9$ was reached, at which the flow between the nozzle exit and the tube inlet switched to the jet screech mode. At this pressure, the free-jet shock location $(X_s/d)_{free\text{-}jet}$ was approximately equal to the tube spacing s/d. Now, a normal shock appeared in front of the tube inlet all the time and oscillated about its mean position. The location of the shock wave in the jet screech mode in Fig. 3 represents its mean position. As the pressure was increased further, the spacing s/d was always less than the free-jet shock location $(X_s/d)_{free\text{-}jet}$. Therefore, the jet flow remained in the jet screech mode.

Also in Fig. 3 are shown the experimental points in the filling phase for the 35.6-cm tube with spacing $s/d = 3.0$. Over the range of pressure investigated, the flow remained in the jet regurgitant mode. The experimental points of shock wave location in the inflow phase X_s/d lie very close to the free-jet location $(X_s/d)_{free\text{-}jet}$, further confirming the conclusions drawn above.

The experimental results for different tube lengths indicating the demarkation line between jet regurgitant and screech modes are shown in Fig. 4. The results of the first and second free shock location $(X_s/d)_{free\text{-}jet}$ are compared with those obtained by Westley and Woolley (Ref. 16). As is clear from Fig. 4, the present results indicated that the shock waves were located farther downstream of the nozzle exit when compared to the data of Westley and Woolley for a given pressure. The experimental results reported herein were derived from free-jet shadowgraphs. Therefore, one cannot expect exact agreement. Along the first free-jet shock locations are

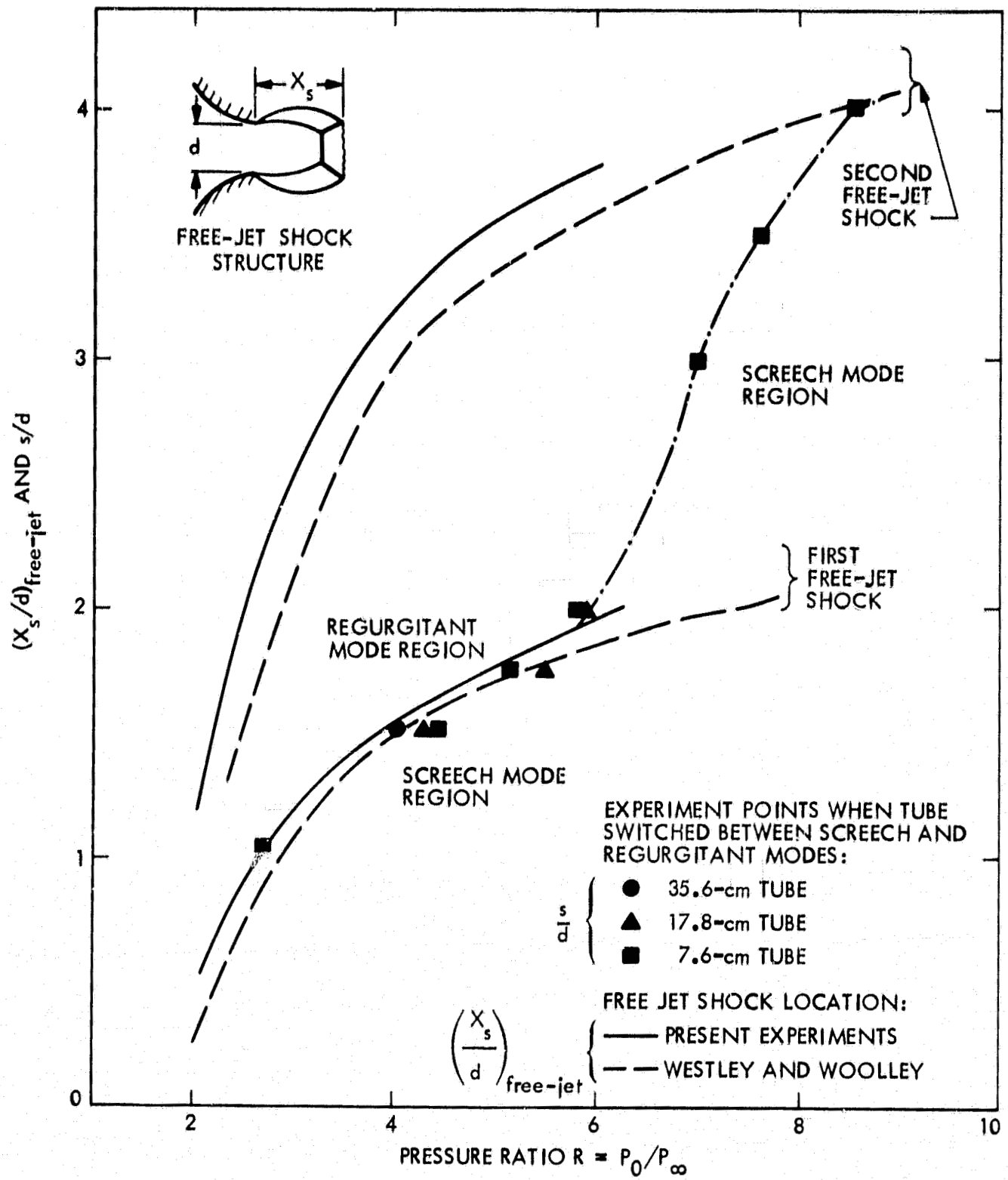

Fig. 4. Regions of resonance tube operation

indicated the spacings s/d at which the jet flow between the nozzle and the resonance tube inlet switched between jet screech and jet regurgitant modes. The experimental points for the various tube lengths lie very close to the first free-jet shock location, confirming the fact that the jet-flow switch between the regurgitant and screech mode occurred at a pressure for which the spacing s/d was approximately equal to the corresponding first free-jet shock location; i.e., $s/d \approx (X_s/d)_{free\text{-}jet}$.

As the pressure ratio R was increased beyond 6, the experimental points when the switch between jet regurgitant and screech modes occurred did not follow the free-jet shock location $(X_s/d)_{free\text{-}jet}$ (Fig. 4). In fact, the switch to the screech mode occurred at larger tube spacing s/d until the tube came into the influence of the second free-jet shock at a pressure ratio $R \approx 8.4$. In Fig. 4, these points have been joined by a dotted line which separates the jet regurgitant and screech modes. It should be noted that the various regions of resonance tube operation were independent of the length of the tube.

It was also observed that in the jet screech mode the almost normal shock wave in front of the tube inlet oscillated in various bands of frequencies depending upon the pressure ratio R and the spacing s/d (see Fig. 21). The effects of various stages of shock wave oscillation in the jet screech mode are discussed in subsequent sections. Also note that the various modes of resonance tube flows discussed above pertain to the interaction of the first free-jet shock cell structure with the tube inlet. Similar results were observed when the tube was placed in other shock cells.

B. VISUALIZATION OF RESONANCE TUBE FLOWS

Spark shadowgraph pictures of the resonance tube flows were undertaken. The density gradient caused by the expansion of nitrogen gas through the nozzle and compression across the shock waves was employed to acquire the shadow effect. A critical examination of the spark shadowgraphs under various flow conditions, as discussed below, provided further insight into the mechanism of gas heating in resonance tubes.

1. Free-Jet Flow Visualization

The free-jet flows were observed over a range of nozzle pressures at which the resonance tubes were studied. As indicated above, the behavior of the free jet is closely related to resonance tube operation in various modes. The effect of tube location in the resonance tube system with respect to that of the free-jet shock is shown in Figs. 3 and 4. This information is useful in the design of a resonance tube system for a particular mode of operation.

In this study, both subsonic and underexpanded supersonic jet flows from a convergent nozzle were examined. Typical shadowgraphs of the free jet at various nozzle pressure ratios are shown in Fig. 5. For nozzle pressure ratios $R \lesssim 1.9$, the jet was subsonic. For $R > 1.9$, the flow was underexpanded and resulted in the formation of shock waves downstream from the nozzle exit. Within the nozzle pressure ratios $1.9 < R < 3.4$, the diamond shock structure was observed. For pressures $R > 3.4$, the well-known "Mach disc" appeared across the jet axis. The strength of this normal Mach disc as well as its distance from nozzle exit increased as the nozzle pressure ratio R was increased.

Large lateral motion of the whole jet flow was observed in the range of pressure ratios $1.9 < R < 3.4$ when the diamond shock structure was observed. The oscillation frequency of this lateral motion of the whole jet resulted in large jet spreading which seemed to have a helical motion. A large spreading of the free jet is seen in the instantaneous shadowgraph in Fig. 5 at a nozzle pressure ratio $R = 2.87$.

2. Shadowgraphs of Resonance Tube Flows at Different Nozzle Pressures

a. Flow Between Nozzle Exit and Tube Inlet at $s/d = 3$. Sequences of instant spark shadowgraphs for the 35.6-cm resonance tube with spacing $s/d = 3$, indicating the jet flow between nozzle exit and tube inlet at various nozzle pressures, are shown in Fig. 6. The flow in these pictures was from left to right. The shadow at the top left in Fig. 6A was that of the triggering microphone which was placed in such a way as not to disturb the jet flow. These instantaneous shadowgraph pictures in Fig. 6 were taken at random and have been put in order of increasing time duration of a typical resonance

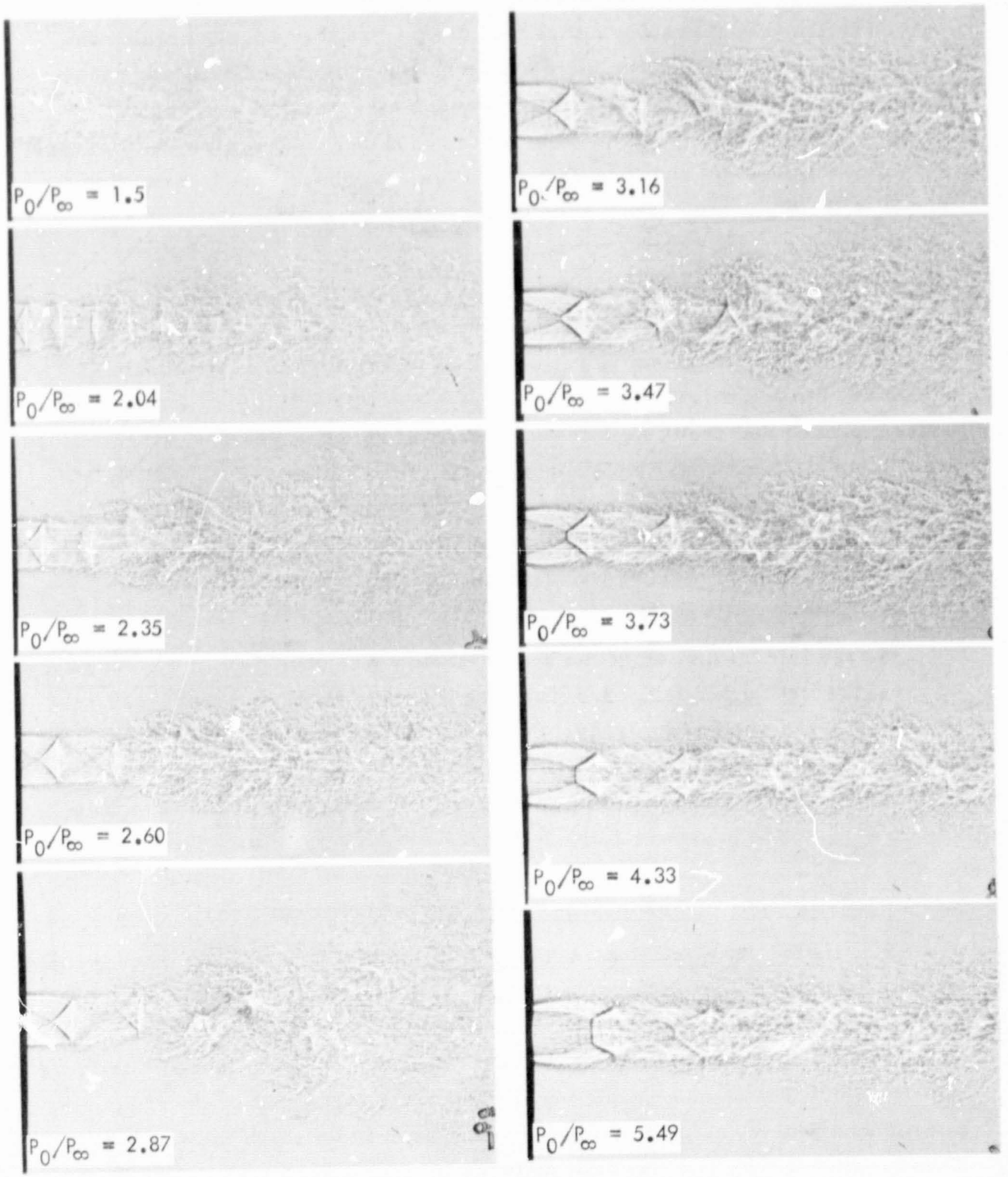

Fig. 5. Free-jet shadowgraph pictures at different nozzle pressure ratios R

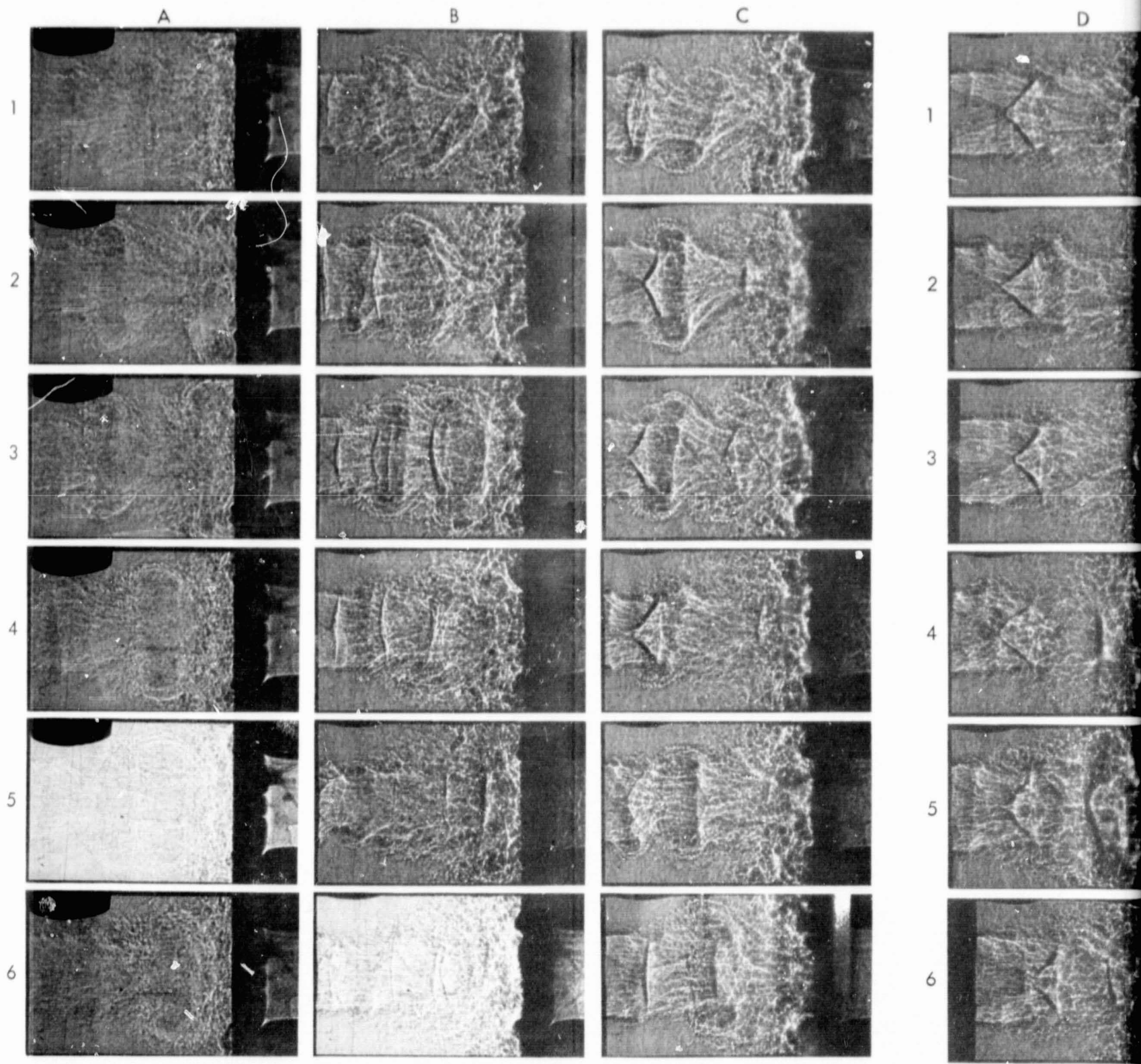
A
B
C
D
1
2
3
4
5
6
P_0/P_∞ = 1.23
P_0/P_∞ = 2.04
P_0/P_∞ = 2.60
P_0/P_∞ = 3.1

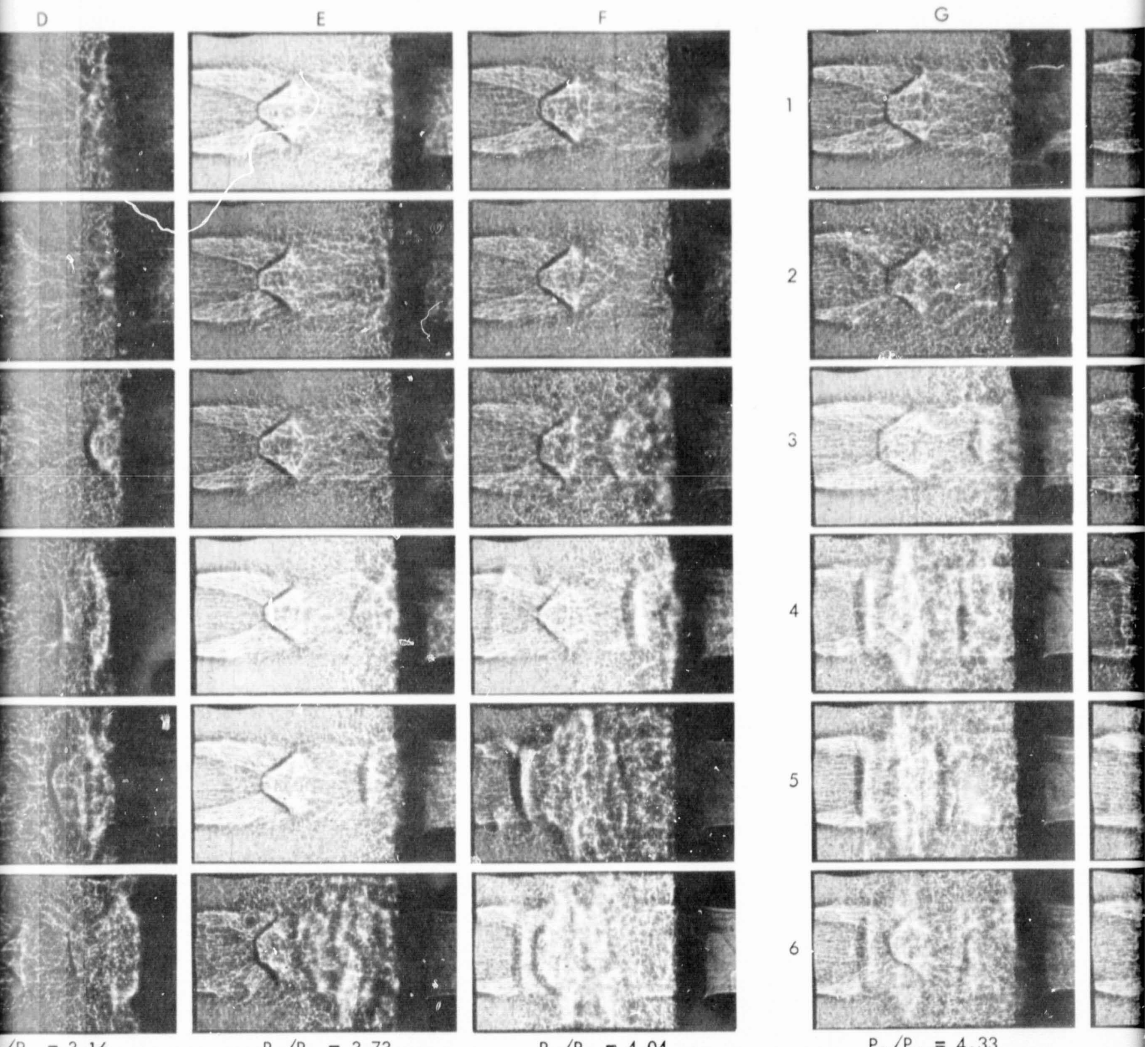

Fig. 6. Sequence of jet-flow shadowgraph pictures of 35.6-cm resonance tube at different

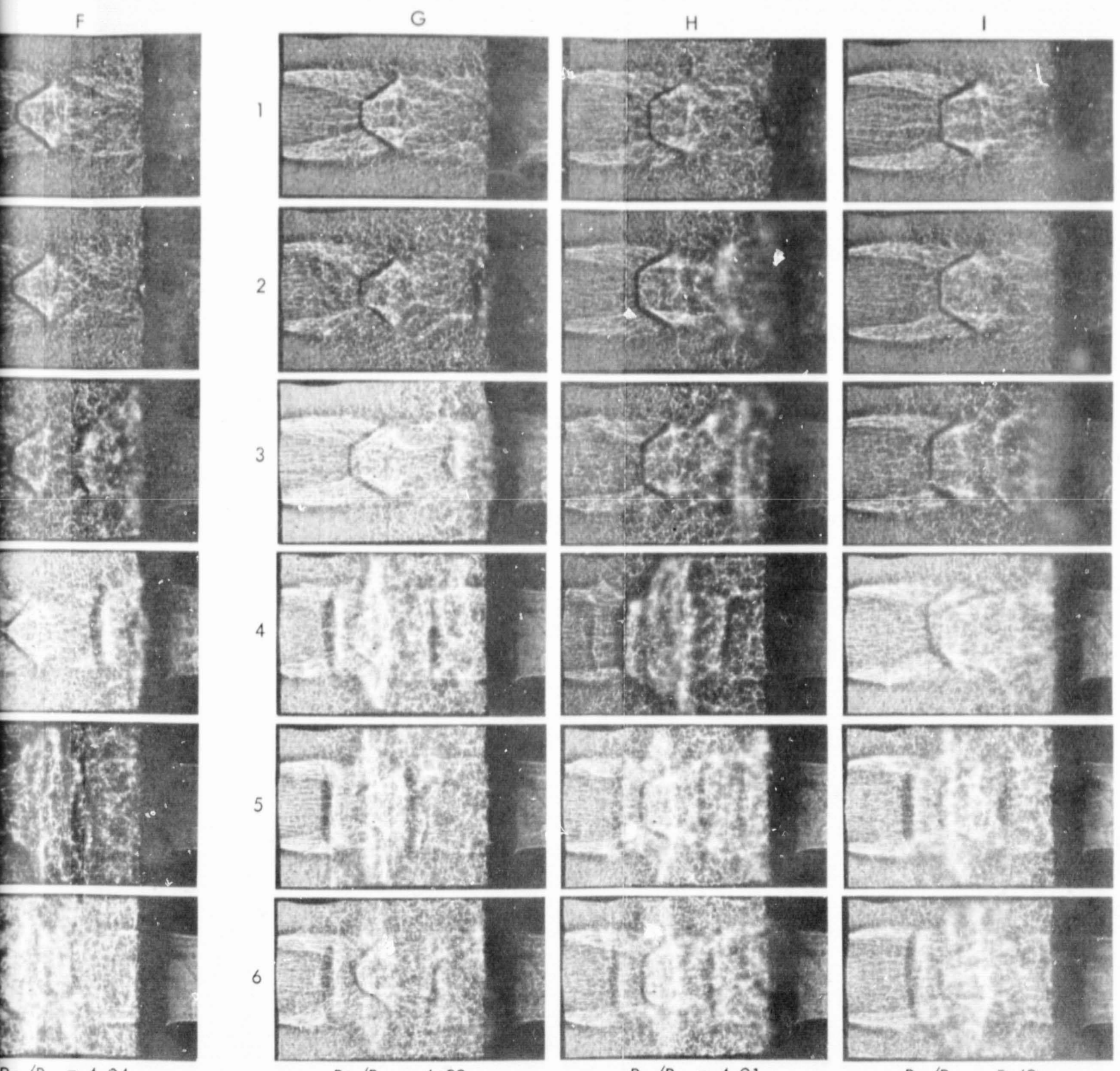

adowgraph pictures of 35.6-cm resonance tube at different nozzle pressure ratios R with spacing s/d = 3

FOLDOUT FRAME

tube cycle from top downwards. The corresponding endwall pressure traces, which are discussed in Section IIIC, are indicated in Fig. 10.

In this section, the various resonance tube modes will be referred to as first or second mode of tube operation, depending upon the interaction of the resonance tube inlet with the first or second free-jet shock cells, respectively.

The jet flow in shadowgraph 6A at a pressure ratio R = 1.23 with spacing s/d = 3 was subsonic. Toroidal vortices shed from the nozzle exit can be seen in these pictures. These vortices grew in size as they propagated toward the resonance tube. The frequency of the vortices scaled as $fd/U_j \simeq 0.3$ to 0.4. On interaction with the tube inlet, the toroidal vortices resulted in periodic waves in the tube at their shedding frequency. At certain subsonic jet flows, the endwall pressure traces indicated the shedding frequency of these toroidal vortices superimposed on the tube resonance frequency $f \simeq a/4L$. As the nozzle pressure was increased beyond R > 1.9, the nozzle flow became underexpanded and resulted in the formation of diamond shock cells (Figs. 6B and 6C). For slightly underexpanded nozzle flows, these toroidal vortices could also be seen in the outer part of the jet shear layer. For nozzle pressure ratios $1.9 < R \lesssim 3.10$, the tube flow alternately switched between the jet screech and regurgitant modes. Under these conditions of flow and tube geometry, the resonance tube was influenced by the various shock cells. Shadowgraph pictures in Figs. 6B and 6C clearly indicated more than one shock cell in the jet flow between the nozzle and the tube.

At a nozzle pressure ratio R = 3.16, the jet flow began to oscillate in the second jet regurgitant mode. Figure 6D, from top downwards, represents the series of jet flow shadowgraphs with increasing time during the jet regurgitant mode cycle. In photograph 6D-1, the jet flow was in the filling phase of the jet regurgitant mode. Most of the jet flow entered the tube. Figure 6D-2 shows the end of the filling phase. The jet flow then switched to the tube efflux phase, which resulted in the formation of an interface between the nozzle jet flow and the tube jet flow. As the outflow phase developed, this interface moved toward the nozzle and resulted in strengthening of the second shock in the nozzle jet flow (Figs. 6D-2 through 6D-5).

The first shock cell in the nozzle jet flow was not much disturbed as the resonance tube went through a cycle of the second jet regurgitant mode. With increasing time, the tube jet flow weakened and the jet flow between the nozzle and the tube switched suddenly back to the filling phase (Fig. 6D-1). This sequence of behavior in the jet flow occurred at the resonance tube fundamental frequency $f \simeq a/4L$.

Similar resonance tube behavior was observed in the sequence of shadowgraph pictures in Fig. 6E for the 35.6-cm resonance tube with spacing $s/d = 3$. The nozzle pressure ratio was $R = 3.73$. The resonance tube flow was in the second jet regurgitant mode.

As the pressure was increased further, the resonance tube flow went into the first jet regurgitant mode. These two regurgitant modes associated with the first and second free-jet shock cells were separated by a small range of pressure ratio at which the resonance tube operated in the second jet screech mode. Figures 6F, G, H, and I represent the sequence of shadowgraph pictures of the jet flow in the first jet regurgitant mode at nozzle pressure ratios of $R = 4.04$, 4.33, 4.91, and 5.49, respectively. For example, at a pressure ratio of $R = 4.91$ (Fig. 6H), the jet flow was initially in the filling phase of the tube (Fig. 6H-1). After completion of the filling phase, the tube jet flow began. This resulted in the formation of an interface between the nozzle jet and the tube jet flows. With increasing time, this interface moved from the tube inlet toward the nozzle (Figs. 6H-2, 3, and 4). Figures 6H-4, 5, and 6 represent the jet in the outflow phase. Two normal shock waves on either side of the interface are evident indicating the two jet flows to be supersonic. These shock waves were moving in the opposite direction with respect to the local gas flows. The strength of this almost normal shock wave between the nozzle exit and the interface changed with time, accompanied by the formation of another shock wave between the normal shock wave and the interface. It also appears from these shadowgraphs (in outflow phase of the jet regurgitant mode) that this third shock appeared randomly in varying strength and location with respect to the interface. As compared to Figs. 6D and 6E, where the tube flow was in the second jet regurgitant mode, the interaction of the nozzle jet and the tube jet flows was much stronger in the first jet regurgitant mode (Figs. 6F, G, H, and I). As will be discussed in Section IIID, this resulted in stronger

shock waves inside the tube and consequently in higher endwall gas temperatures.

b. Flow Inside Tube at s/d = 3. Instant shadowgraphs indicating the tube flow as well as the jet flow between the nozzle exit and the tube inlet for the 35.6-cm tube with spacing s/d = 3 are shown in Fig. 7. These pictures were studied along with the sequence of jet flow pictures shown in Fig. 6. Figures 7A and B represent the resonance tube in the jet instability mode where toroidal vortices were shed in the jet flow from the nozzle exit, resulting in the generation of a train of very weak shock waves inside the tube at the shedding frequency of these vortices. For slightly underexpanded jet flows (Figs. 7C and D), these toroidal vortices could be seen in the jet along with multiple shock cells. Under these flow conditions, the tube was operated by these diamond shock cells at relatively high frequencies as compared to the fundamental tube resonance frequency. Multiple weak wavefronts were generated inside the tube. With increasing pressure, the jet flow began to oscillate in the second jet regurgitant mode. The flows in Figs. 7E and F represent the tube flow in the outflow phase of the jet regurgitant mode. The first and second shocks, along with the interface in the jet flow between the nozzle exit and the tube inlet can be seen (Fig. 7F). No shock waves of significant strength occurred inside the tube flow in the outflow phase (Figs. 7D to F).

Flows in Figs. 7G, H, I, J, and K represent the resonance tube flow in various phases of the first jet regurgitant mode. Large turbulent flow close to the tube inlet was observed during the inflow phase as seen in Fig. 7G. This large turbulent fluid motion is believed to have been caused by the interaction of the impinging nozzle jet flow with the tube inlet. This jet inflow resulted in the formation of an incident shock wave followed by a contact surface. This incident shock wave can be seen travelling toward the endwall in Fig. 7G and resulted in heating the tube gas by dissipative processes across it. The contact surface travelled toward the endwall (behind the incident shock) and divided the tube gas and the nozzle jet flow. The incident shock wave reflected from the endwall and on interaction with the contact surface (which was moving towards the endwall) resulted in strong turbulent mixing. This phase of the jet regurgitant mode is shown in Fig. 7H. The reflected wave is not visible in Fig. 7H, though the

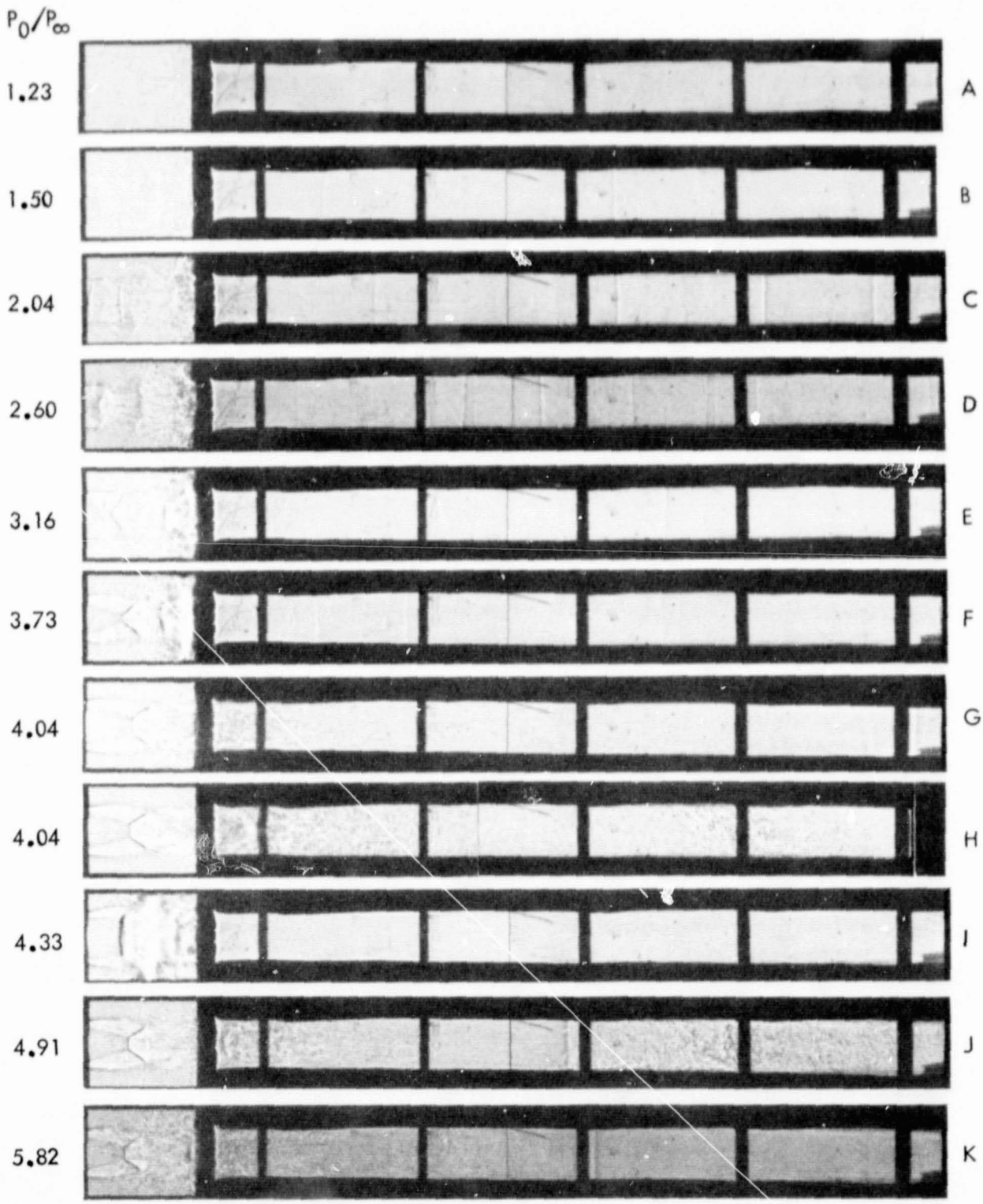

Fig. 7. Sequence of snadowgraph pictures of 35.6-cm resonance tube at different nozzle pressure ratios R with spacing s/d = 3

turbulent mixing can easily be seen. The reflected shock wave is probably hidden behind the shadow of the bolt. Figure 7J represents similar flow condition at nozzle pressure ratio R = 4.91 and clearly indicates the reflected shock wave along with the turbulent mixing caused by the interaction of this wave with the contact surface. It should also be noted that as the reflected shock wave moved away from this plane of interaction, the flow behind the reflected wave was less turbulent. These shadowgraphs (Figs. 7G and J), showing large turbulent fluid motion on collision of the contact surface with the reflected shock wave, strongly suggest that large periodic mixing and exchange of mass between cold nozzle jet flow and the oscillating hot tube flow occurs during the inflow phase. The instant shadowgraph in Fig. 7I represents the tube flow at a nozzle pressure ratio R = 4.33, in the outflow phase of the jet regurgitant mode. The interaction of the nozzle and the tube jet flows with the interface in between is evident. The flow inside the tube in this part of the cycle was free of turbulent mixing and of shock waves since only expansion waves existed. These did not result in any abrupt changes in flow and consequently did not have any strong shadow effect. Figure 7J represents the tube flow as in Fig. 7H discussed above. At nozzle pressure R = 5.82, the flow in Fig. 7K represents the beginning of the inflow phase. Turbulent mixing can be seen near the inlet of the tube. One can also see the formation of an incident shock wave which was travelling towards the endwall of the tube. As expected, the tube flow in front of this incident shock wave was free of turbulent mixing.

The sequences of shadowgraphs in Figs. 6 and 7 were not taken at high enough nozzle pressure ratios R to operate the resonance tube with spacing s/d = 3 discussed above in the jet screech mode. The following results will shed some light on this mode of resonance tube operation.

c. Flow Between Nozzle Exit and Tube Inlet at s/d = 1.5. A sequence of shadowgraph pictures for the 35.6-cm resonance tube with spacing s/d = 1.5 is shown in Fig. 8. Like the shadowgraphs in Fig. 6, these pictures were taken randomly and have been arranged in sequence of increasing time (from the top downward) of a typical resonance tube cycle. These shadowgraphs show the jet flow along with the flow close to the inlet of the resonance tube. At a nozzle pressure ratio $R < 1.9$ (Fig. 8A), the resonance tube was in the jet instability mode. No large

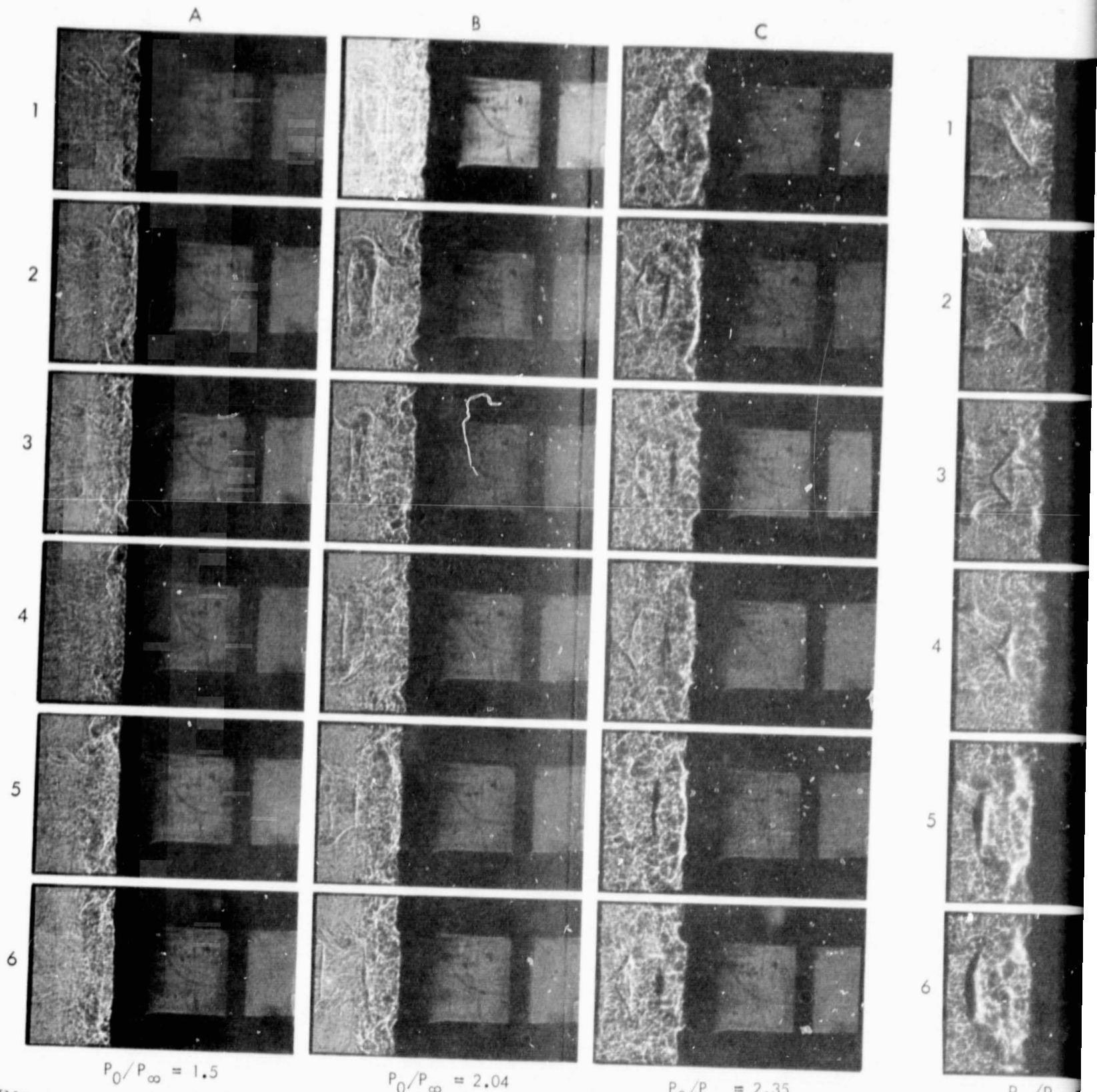

PRECEDING PAGE BLANK NOT FILMED

FOLDOUT FRAME 1

ORIGINAL PAGE IS
OF POOR QUALITY

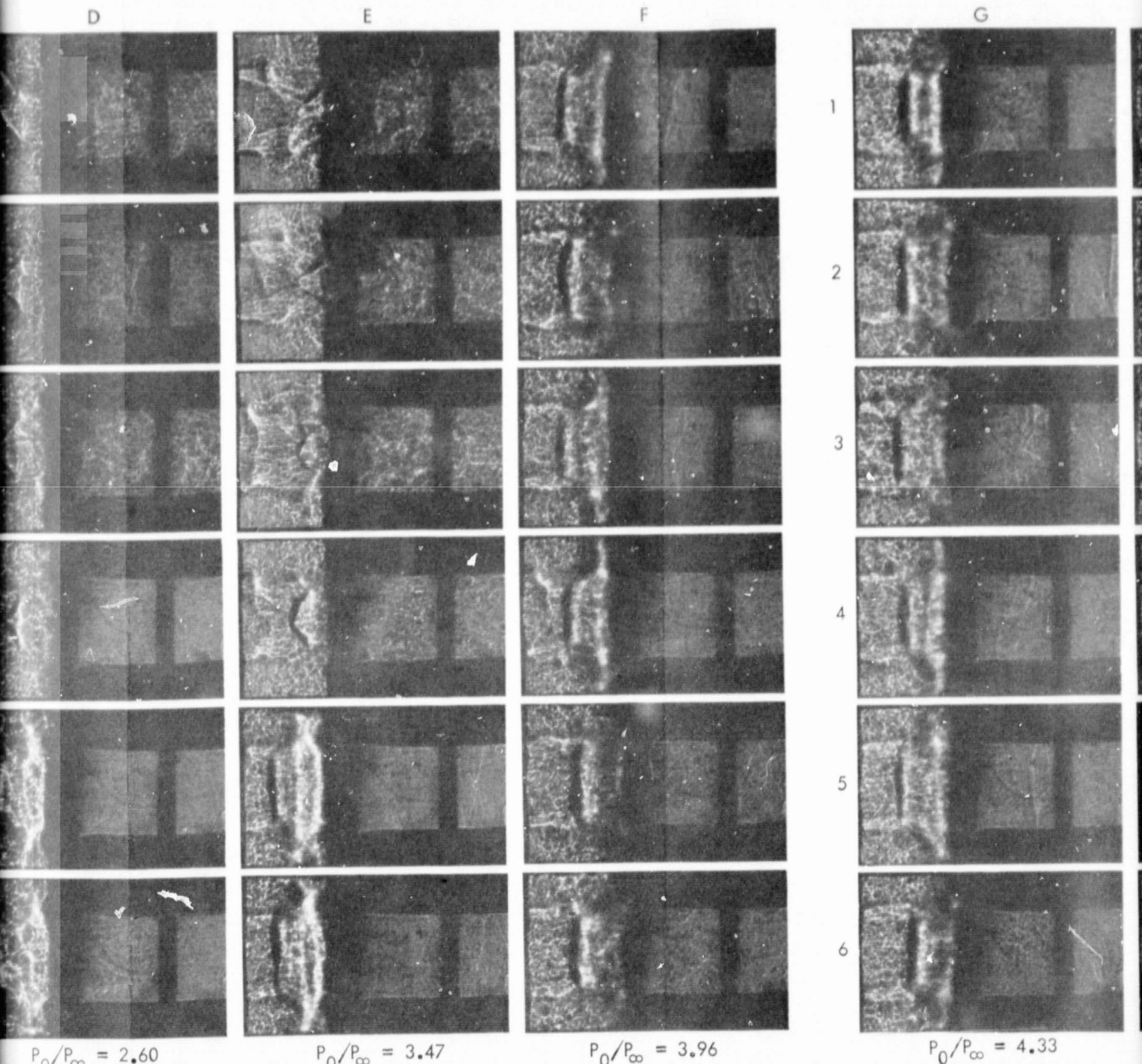

Fig. 8. Sequence of jet-flow shadowgraph pictures of 35.6-cm resonance tube at differe

FOLDOUT FRAME 2

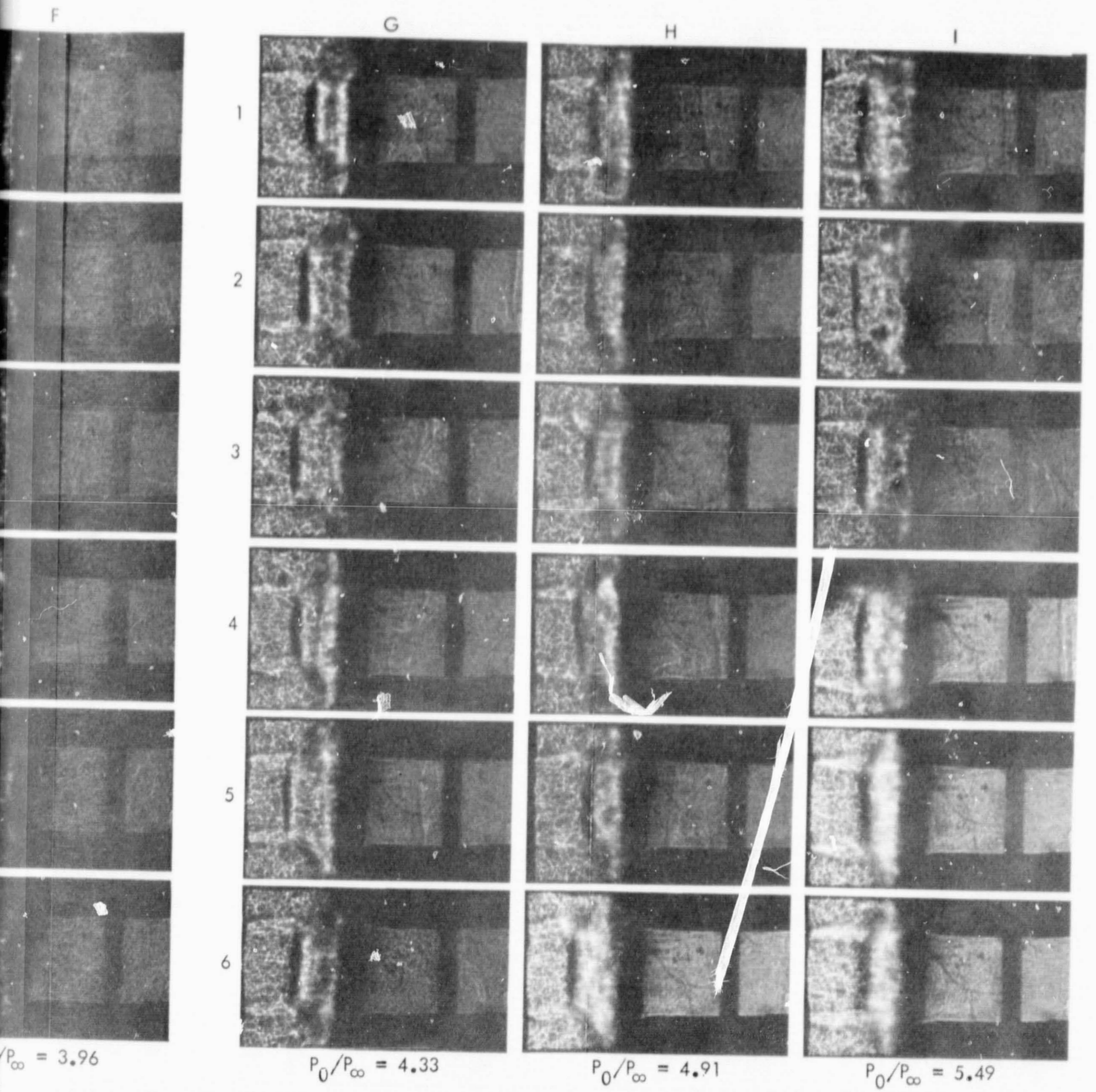

graph pictures of 35.6-cm resonance tube at different nozzle pressure ratios R with spacing s/d = 1.5

FOLDOUT FRAME 3

pressure fluctuations at the endwall of the tube occurred in this mode of operation. As the jet flow became slightly underexpanded with R = 2.04 (Fig. 8B), the tube was in the jet screech mode of operation due to the influence of the multiple diamond shocks. Both in the jet instability mode and in the slightly underexpanded jet screech mode of operation, weak compression wave fronts were observed along the resonance tube. Shadowgraphs in Fig. 8C represent the flow in second jet screech mode. These figures clearly show a normal shock wave which always stood in front of the tube inlet. The first shock location and its strength did not change with time in this case.

At a nozzle pressure ratio of R = 2.60 (Fig. 8D), the jet flow went into the regurgitant mode associated with the first shock cell. Figures 8D-1, 2, and 3 represent with increasing time the inflow phase of jet regurgitant mode. There was considerable turbulent fluid motion close to the tube inlet in this phase of the regurgitant mode when most of the nozzle jet flow entered the tube. The jet structure in the filling phase was quite independent of the presence of the tube. Figure 8D-4 represents the outflow phase. In this phase, as one would expect, no mixing close to the tube inlet occurred. As the tube jet flow gathered strength, an interface was formed which moved from the tube inlet toward the nozzle exit. This resulted in strengthening of the nozzle shock, which became almost a normal shock as it moved toward the nozzle exit (Figs. 8D-5 and 6).

The sequence of shadowgraphs in Fig. 8E, at nozzle pressure R = 3.47, shows the jet regurgitant mode similar to Fig. 8D. In these pictures, the interface can be seen very clearly in the outflow phase of the regurgitant mode (Figs. 8E-5 and 6). As the pressure was increased beyond R ≳ 3.9, the jet flow switched to the jet screech mode for the 35.6-cm resonance tube with s/d = 1.5.

Typical shadowgraphs of the jet flow in the screech mode at a nozzle pressure R = 3.96 are shown in Fig. 8F. As pointed out earlier, a normal shock which oscillated at high frequency as compared to the fundamental resonance tube frequency for this tube (which was approximately 250 Hz) always stood in front of the resonance tube inlet. The screech frequency was approximately 4 kHz and increased slightly with increasing nozzle

pressure ratio. By noting the flow close to the resonance tube inlet, it is apparent that very little nozzle jet flow entered the tube compared to the inflow phase of the jet regurgitant mode. As will be discussed subsequently, weak shock waves (as compared to the jet regurgitant mode) were observed at the oscillation frequency of this normal shock, which always stood in front of the tube. Jet flows in Figs. 8G, H, and I represent the jet screech mode at higher nozzle pressure ratios R.

d. Flow Inside Tube at s/d = 1.5. Shadowgraphs of the resonance tube and jet flows at various nozzle pressures of the 35.6-cm resonance tube with spacing s/d = 1.5 are shown in Fig. 9. In Fig. 9A the subsonic jet flow and the train of waves inside the tube were at the frequency of the toroidal vortices shed from the nozzle exit. At a pressure ratio R = 2.04, the tube was under the influence of the second diamond shock. With increased nozzle pressure, as discussed previously, the jet flow switched to the jet regurgitant mode. Figure 9C represents the resonance tube flow in the inflow phase of the jet regurgitant mode. Considerable turbulent flow can be seen close to the inlet of the tube. Figure 9D at R = 3.16 represents the outflow phase of the regurgitant mode and does not show large irregular motion close to the inlet of the tube.

For a nozzle pressure ratio ≥ 3.96, the resonance tube went into the jet screech mode. This resulted in the formation of an almost normal shock which in turn resulted in a train of weak shock waves inside the tube at the frequency of its oscillations. The flows in Figs. 9E, F, G, H, and I represent the jet screech condition at nozzle pressure ratios of 3.96, 4.04, 4.33, 4.91, and 5.49, respectively. These pictures clearly show multiple wavefronts travelling into and out of the tube. Very little of the nozzle jet flow entered the tube in this mode of operation as compared to that in the jet regurgitant mode in the inflow phase (Fig. 9C).

C. ENDWALL PRESSURE MEASUREMENTS

Endwall pressure measurements were made over a large range of spacings s/d, nozzle pressure ratios, and for different tube lengths with piezoelectric pressure transducers. A study of these traces along with the corresponding endwall gas temperature traces produced further insight into the heating mechanism of the tube gas.

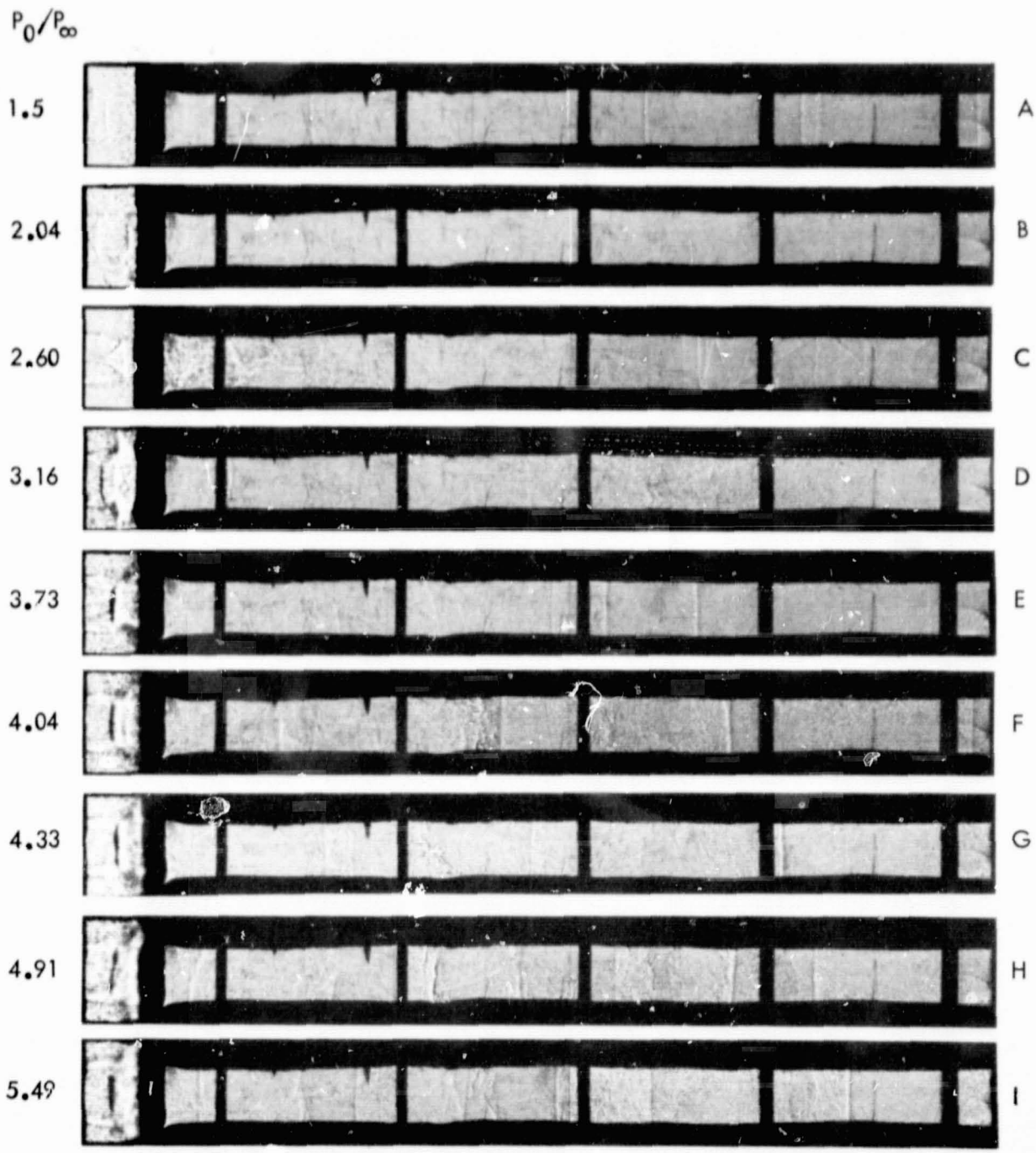

Fig. 9. Sequence of shadowgraph pictures of 35.6-cm resonance tube at different nozzle pressure ratios R with spacing s/d = 1.5

Typical endwall pressure traces for the 35.6-cm lucite resonance tube with spacing s/d = 3 at various nozzle pressures are shown in Fig. 10. In comparing the endwall pressure traces at different nozzle pressures, it should be noted that the vertical and horizontal scales in Fig. 10 are not identical for all the traces. Endwall pressure traces for subsonic jet flows (see traces in Fig. 10 at nozzle pressures R = 1.23 and 1.50) show weak periodic signals. As pointed out above, these waves in the tube were caused by the interaction of the toroidal vortices with the resonance tube inlet. These weak pressure oscillations in the tube did not result in heating the gas near the endwall. For certain nozzle flow and tube configurations, the non-dimensional frequency of the toroidal vortices was observed to be superimposed on the endwall pressure signal at the fundamental resonance tube frequency, i.e., $f \simeq a/4L$.

As the nozzle pressure ratio was increased beyond R > 1.9, the jet flow was underexpanded and, as discussed above (in Section IIIB), resulted in the formation of diamond shock wave cells. At low underexpansion nozzle pressure ratios, the tube with spacing s/d = 3 was excited in the screech mode by these multiple shock wave cells. Typical endwall pressure traces for the jet screech mode excited by multiple shock cells are shown in Fig. 10 at nozzle pressure ratios R = 2.04 and 2.60. At a nozzle pressure ratio R ≃ 3.16, the tube flow went into the second jet regurgitant mode (see the corresponding jet flow between the nozzle exit and the tube mouth in Fig. 6D). One clearly sees the shock wave followed by compression waves in Fig. 10 at R = 3.16. This wave was formed during the inflow phase of the jet regurgitant mode. As this compression wavefront reached the resonance tube inlet after reflection from the endwall (thus completing the inflow phase), it resulted in generation of an expansion wavefront. This wavefront began to travel toward the endwall and resulted in the initiation of the jet outflow phase. During the time it takes for this expansion wavefront to reach the endwall, as is clear from the endwall pressure trace, the pressure remained constant. As the expansion wavefront arrived at the endwall, the endwall pressure decreased and reached the lowest pressure in this cycle of regurgitant mode operation. The outflow phase was completed as the expansion fan reached the resonance tube inlet after reflection from

Fig. 10. Typical endwall pressure traces of 35.6-cm resonance tube at different nozzle pressure ratios R with spacing s/d = 3

the endwall. The tube flow then switched to the jet inflow phase and resulted in a sudden pressure jump across the incident shock followed by compression waves. This cycle took place at the fundamental resonance frequency of the tube. The endwall pressure trace at R = 3.73 in Fig. 10 also represents the resonance tube flow in the jet regurgitant mode excited by the second shock wave cell.

At a nozzle pressure ratio of R = 4.33, the resonance tube began to oscillate in the first jet regurgitant mode. The endwall pressure trace at R = 4.33 indicated a much stronger normal shock wave in the tube compared to the trace at R = 3.16 or 3.73 in Fig. 10. This is expected because the first shock wave cell is much stronger than the second shock wave cell; there is a stronger inflow phase when the tube is placed under the influence of the first shock cell as compared to the second one. The gas temperature in the vicinity of the endwall was higher when the tube was in the first jet regurgitant mode as compared to the second. As the nozzle pressure was increased further (e.g., R = 4.91 and 5.49), the endwall pressure traces showed a reduction in the strength of the shock wave in the compression phase of the jet regurgitant mode and resulted in a reduction of the corresponding endwall gas temperatures.

Typical results of endwall pressure traces for the 17.8-cm resonance tube are indicated in Fig. 11, where the spacing between the nozzle exit and the tube inlet s/d was 2.0. For subsonic jet flows (pressure traces at R = 1.5 and 1.8 in Fig. 11) large toroidal vortices were formed, resulting in relatively weak compression waves as shown in these traces. At a pressure ratio R = 2.04, the endwall pressure trace shows the resonance tube flow in a jet screech mode by the multiple shock cells. For this resonance tube configuration, at a nozzle pressure R = 2.35, the tube flow went to the first jet regurgitant mode. The endwall pressure trace at R = 2.35 in Fig. 11 shows a complete cycle of the endwall pressure trace at the fundamental tube resonance frequency $f \simeq a/4L$. It should be noted in this trace (and also for endwall pressure traces at R = 2.60, 3.16, 3.73, 4.33, 4.91 and 5.49) that the compression phase of the regurgitant mode cycle consisted mostly of a series of small compression wavefronts as compared to formation of shock waves in Fig. 10 at pressure ratio R = 3.16, 3.73,

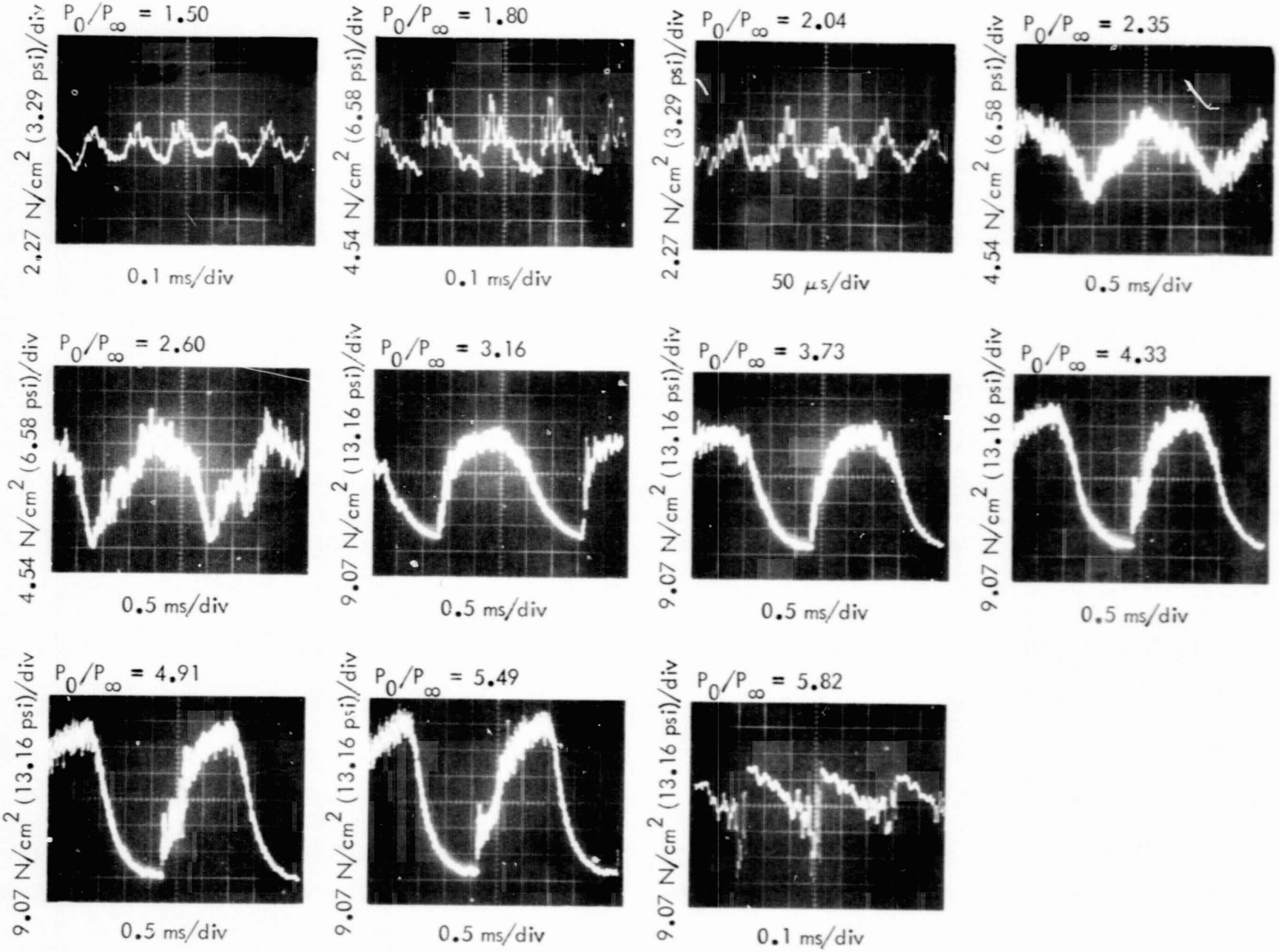

Fig. 11. Typical endwall pressure traces of 17.8-cm resonance tube at different nozzle pressure ratios R with spacing s/d = 2

4.33, etc. On comparing the corresponding endwall temperature traces, lower endwall gas temperatures in the jet regurgitant mode were obtained in flows where weak shock waves were present in the compression part of the endwall pressure trace. These results strongly suggest that heating in the jet regurgitant mode of resonance tube operation was caused mainly by dissipative processes across the shock waves formed inside the tube.

As the pressure was increased further, the resonance tube flow switched to the jet screech mode. The typical endwall trace at nozzle pressure R = 5.82 in Fig. 11 represents the pressure history in the jet screech mode for the 17.8-cm tube with s/d = 2. The endwall pressure traces in the jet screech mode of tube operation showed small-amplitude high-frequency (as compared to jet regurgitant mode) periodic oscillations. As will be discussed in Section IIID, sudden changes in the endwall gas temperature occurred when the resonance tube flow switched from the jet regurgitant to the jet screech mode. This study showed that these high-frequency endwall oscillations were caused by the oscillating normal shock which always existed between the resonance tube inlet and the nozzle exit in the screech mode. Results presented in Section IV showed that very high endwall gas temperatures were obtained when the resonance tubes were tuned to these high-frequency shock wave oscillations in the jet screech mode.

It was also observed that in the jet regurgitant mode of resonance tube operation, the strength of the endwall pressure traces (after the initial transient period) were independent of time; i.e., the strength of the shock waves inside the tube did not change with time.

D. TEMPERATURE MEASUREMENTS IN RESONANCE TUBES

Endwall gas temperatures for various resonance tube flow conditions for which the endwall pressure traces as well as the flow visualization discussed above were measured with 40-gauge chromel-alumel thermocouples (wire diameter 0.0076 cm, 0.003 in.). The output of the thermocouple was recorded on an oscilloscope. A typical endwall gas temperature trace for spacing s/d = 1.75 and pressure ratio R $\simeq$ 6.8 with 7.6-cm resonance tube is shown in Fig. 12. The temperatures referred to in the following section

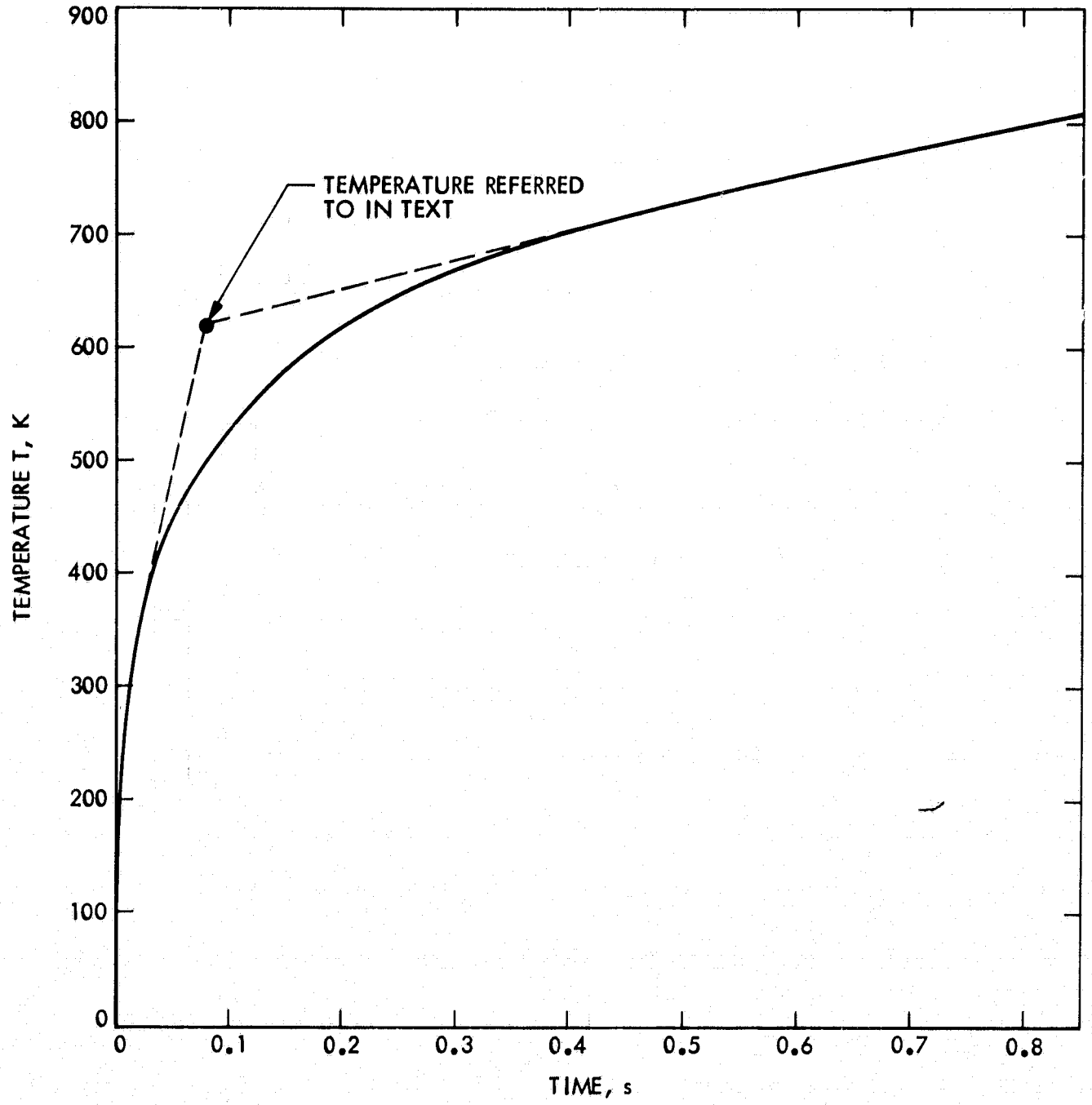

Fig. 12. Typical endwall gas temperature as a function of time for 7.6-cm tube with spacing s/d = 1.75

were defined by taking the intersections of tangents drawn at the initial and the final slopes of the temperature trace as shown in Fig. 12. Most of the temperatures referred to below, therefore, were recorded in less than 100 ms. But the actual rise time of the endwall gas temperature is believed to be shorter than the recorded rise time. This was mainly attributed to thermal inertia of the thermocouple junction and conduction losses to the endwall of the resonance tube. When the highest heating in the resonance tube was attained (approximately 900 K), the tube charred. Thus the highest temperature referred to is only up to the time that tube failure occurred, which was approximately 50 ms or less in these experiments.

1. Endwall Gas Temperature in Various Modes of Tube Operation

The effect of upstream nozzle pressure ratio R on the endwall gas temperature for the 7.6-cm resonance tube with spacings a/d = 1.5, 1.75, 2, and 3 are shown in Fig. 13. As pointed out previously, these temperatures were determined from the intersection of tangents drawn at the initial and the final slopes to the temperature trace. For subsonic flow (pressure ratio $R < 1.9$), the jet flow was in the jet instability mode, during which there was little rise in the endwall gas temperature, as indicated in Fig. 13. For low underexpanded nozzle flows, the flow visualization and endwall pressure traces showed the resonance tube flow in the jet screech mode excited by the multiple shock cells. This resulted in weak compression waves at screech frequency and did not result in significant heating of the gas near the endwall.

The resonance tube flow switched to the jet regurgitant mode at a nozzle pressure R of about 2.40 and remained in this mode up to $R \simeq 4.35$. In the jet regurgitant mode, endwall pressure traces showed oscillations at the fundamental resonance frequency $f \simeq a/4L$, which for this tube was approximately 1000 Hz. The compression part of the endwall pressure trace when the resonance tube flow was in the jet regurgitant mode showed no shock waves. Because of the comparatively short tube length, the compression waves generated by the inflow phase of the jet regurgitant mode had no time to coalesce to form shock waves. Consequently, the rise in temperature which occurred through these trains of compression waves was nearly isentropic. As these compression waves were reflected from the tube inlet

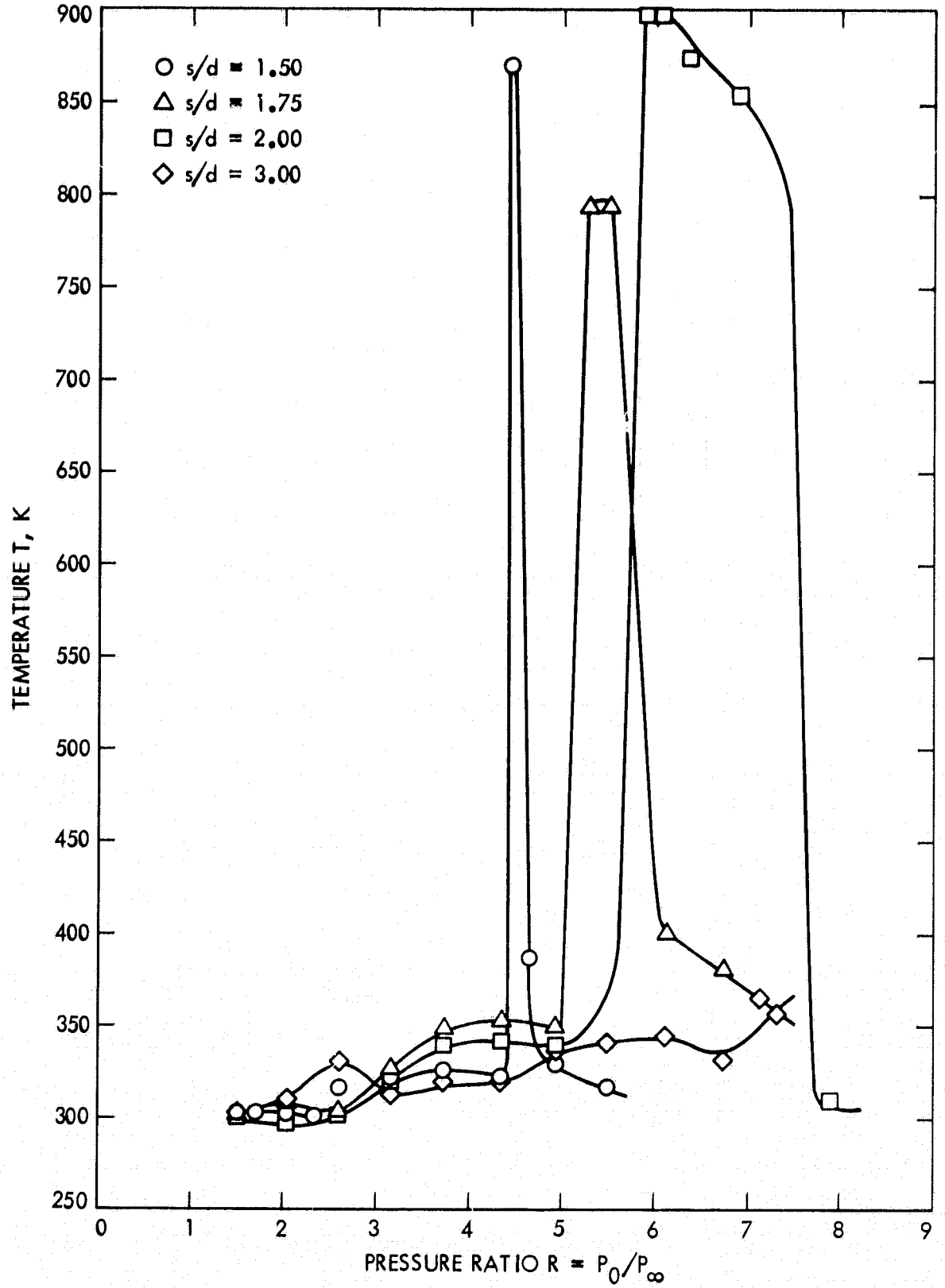

Fig. 13. Effect of nozzle pressure ratio R on endwall gas temperature for 7.6-cm resonance tube

as expansion waves (at the end of the inflow phase), the endwall tube gas was cooled back to the initial temperature isentropically. No significant heating resulted, therefore, in the regurgitant mode cycle. Since the response time of the thermocouple was 50 ms or less, it was reading a mean temperature in this cycle. The time period of 1 ms for the jet regurgitant mode cycle of the 7.6-cm tube was very small compared to thermocouple response time. For these short tubes, hardly any increase in endwall gas temperature was increased in the jet regurgitant mode as indicated in Fig. 13.

At a nozzle pressure ratio of about $R \simeq 4.35$, the jet tube switched to the jet screech mode. As soon as the tube flow switched to the screech mode, the endwall gas temperature suddenly rose to approximately 870 K and resulted in the charring of the lucite walls of the resonance tube. As the nozzle pressure was increased a little further, as shown in Fig. 13, the gas temperature decreased suddenly almost to room temperature. This drastic heating and abrupt cooling of the endwall gas with a change in nozzle pressure ratio was also observed by Sprenger (Ref. 8). These effects will be discussed in detail in Section IV.

The general behavior of the endwall gas temperature for other spacings s/d with nozzle pressure ratio for the 7.6-cm resonance tube was identical with that explained above for $s/d = 1.5$. The two main features were that with increased spacing the switch from jet regurgitant to jet screech mode occurred at high nozzle pressures. The range of pressure over which this intense heating occurred (with tube failure) increased as shown in Fig. 13. For a spacing $s/d = 3$, no intense heating zone was observed over the range of nozzle pressures tested because the tube flow remained in the jet regurgitant mode.

The experimental results of the endwall gas temperature for the 17.8-cm resonance tube with spacing $s/d = 1.5$, 2, 3 and 4 are indicated in Fig. 14. No significant heating for spacing $s/d = 1.5$ resulted for subsonic and slightly underexpanded jet flows. As the flow went to the jet regurgitant mode at approximately $R \simeq 2.4$, there was a little more heating of the endwall gas for this tube flow than for the 7.6-cm tube. The small heating may be attributed to formation of shock waves in the inflow phase of the jet regurgitant mode. This was due to increased tube length, which allowed the

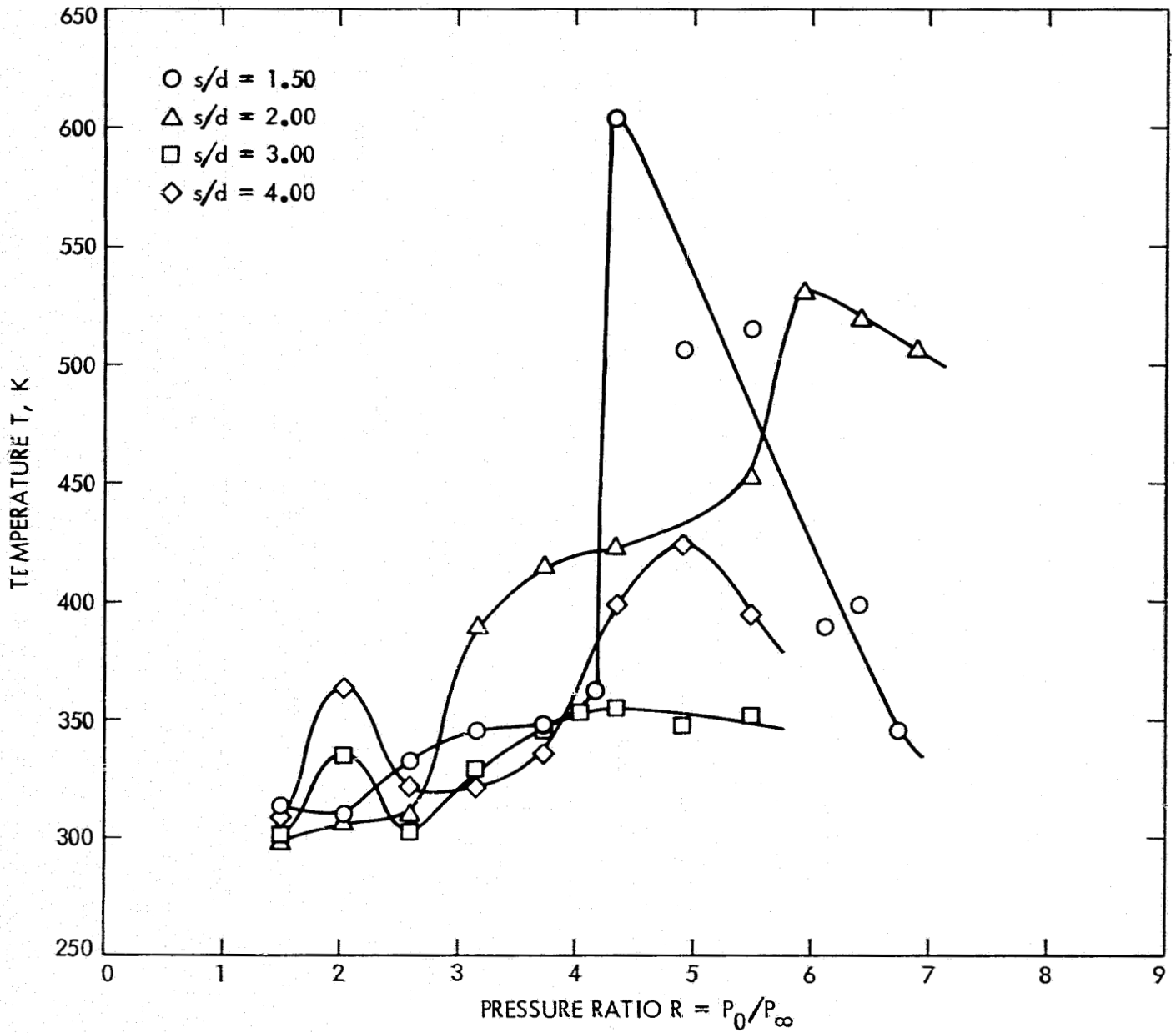

Fig. 14. Effect of nozzle pressure ratio R on endwall gas temperature for 17.8-cm resonance tube

compression waves to coalesce and form the shock wavefront. These resulted in the generation of heat by dissipative processes across the shock waves formed in the tube (increased entropy), leading to an increase in the endwall gas temperature.

The tube flow switched to the jet screech mode at a nozzle pressure ratio of approximately R ≃ 4.3, and this resulted in a sudden increase in endwall gas temperature, which then decreased with increasing pressure ratio. The rise in temperature for the 17.8-cm resonance tube with spacing s/d = 1.5 was not as large as for the 7.6-cm resonance tube (with same spacing) when the resonance tube flow switched from jet regurgitant to jet screech mode at the same nozzle pressure ratio. It should be noted that the demarcation line among various modes of operation was independent of the resonance tube length L. For other spacing (s/d = 2 and 3 in Fig. 14), another small peak in endwall gas temperature was observed for slightly underexpanded jet flows. This was due to tube operation in the jet regurgitant mode by the second shock. For spacing s/d = 2, in the jet regurgitant mode of operation by the first shock, considerably higher endwall gas temperatures were obtained as compared to s/d = 1.5 in Fig. 14. Study of endwall pressure traces showed stronger shock waves for the same nozzle pressure ratio with spacing s/d = 2 as compared to s/d = 1.5. As the nozzle pressure was increased for s/d = 2, the jet flow switched to the jet screech mode with an increase in endwall gas temperature. No significant heatings of endwall gas temperature were observed for spacings s/d = 3 and 4 in jet regurgitant mode over the range of nozzle pressure ratios investigated.

The results in Fig. 15 represent the endwall gas temperature in the 35.6-cm resonance tube with spacings s/d = 1.5, 3, and 4 at various nozzle pressures. As compared to shorter tubes, considerably higher endwall gas temperatures were obtained in the jet regurgitant mode. These were mainly due to stronger shock wave formation inside the tube in the inflow phase of the regurgitant mode. For spacing s/d = 1.5, as the tube flow switched to screech mode at nozzle pressure R ≃ 4.3, there was a small drop in endwall gas temperature. Under identical flow and tube spacing, it should be recalled that the 7.6-cm tube showed a temperature of about 870 K in Fig. 13. For larger spacings s/d = 3 and 4, higher endwall gas temperatures were obtained in the jet regurgitant mode as compared to spacing s/d = 1.5. Thus it was

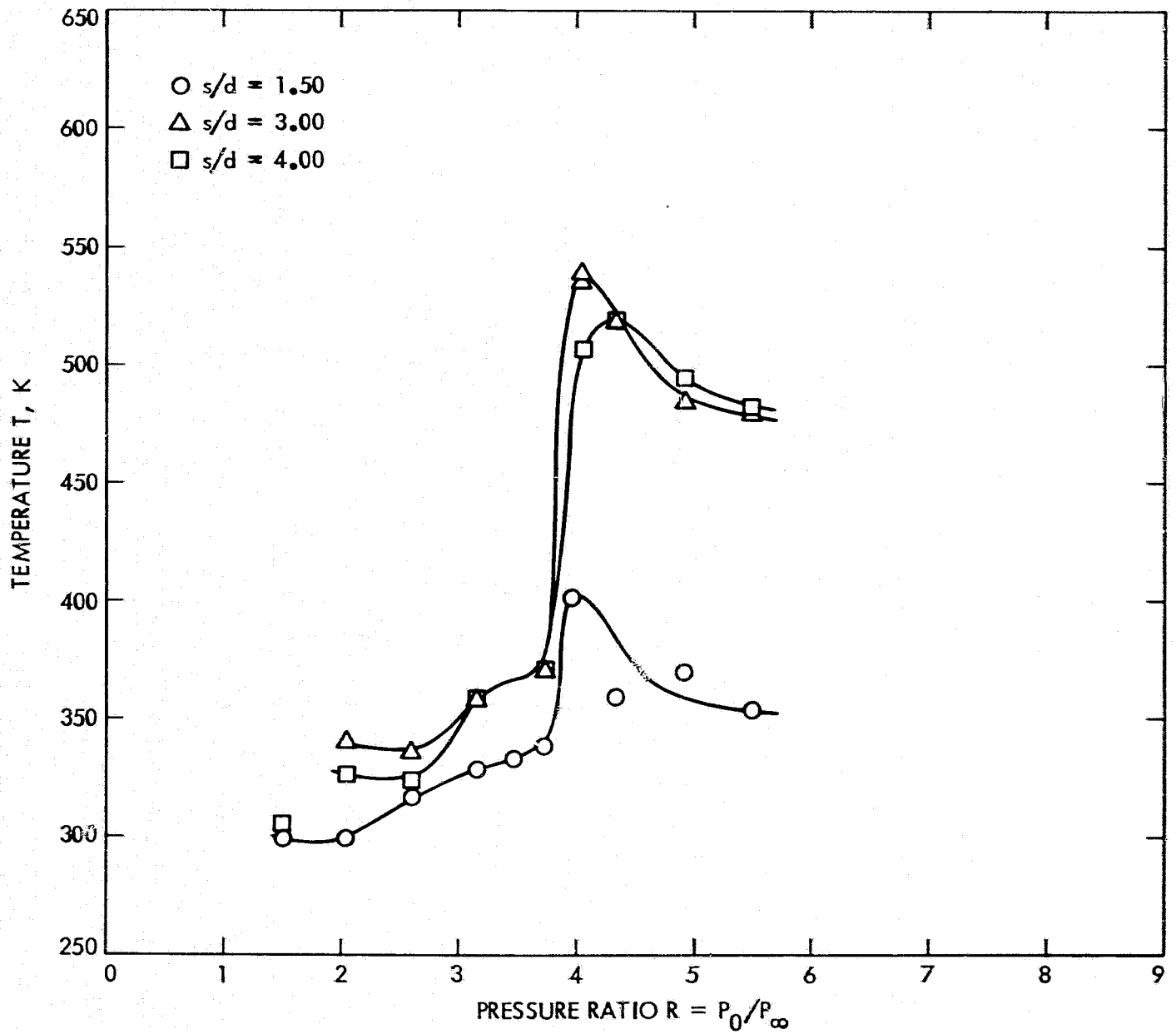

Fig. 15. Effect of nozzle pressure ratio R on endwall gas temperature for 35.6-cm resonance tube

concluded that the length of the tube played a key role in endwall gas temperature both in the jet screech and the jet regurgitant modes.

2. Sidewall Tube Temperature

Temperatures on the external surface of the 35.6-cm-long stainless steel tube were measured along with the endwall gas temperature (see Table 1). Typical results are shown in Figs. 16 and 17. The measurements under identical spacing and nozzle pressure ratios as for the square cross-sectional lucite tube showed that the endwall gas temperatures were almost similar. The sidewall tube temperatures for various nozzle pressure ratios with spacing $s/d = 1.5$ are shown in Fig. 16. In comparing the endwall gas temperatures in Fig. 16 with those of the square cross-sectional lucite tube shown in Fig. 15, it should be pointed out that the data for the steel tube represent the temperature attained at the end of the typical run, which was as long as half a minute. Endwall tube temperatures were also measured, and it should be noted that the endwall gas temperatures were considerably higher than these, as one would expect. The drop in sidewall tube temperature close to the end of the tube was due to heat conduction losses from the tube endwall to the vertical plate holding the resonance tube (Fig. 1). Similar sidewall tube temperatures with spacing $s/d = 3$ at various nozzle pressure ratios are shown in Fig. 17. Over the range of nozzle pressure ratios at which these tests were performed, $1.5 < R < 5.49$, the resonance tube was operating in the jet regurgitant mode. It should be noted that about 60% of the tube was not heated at all. Most of the heating of the tube occurred near the endwall.

To determine the importance of sidewall heat conduction losses on endwall gas temperature, experiments were performed on the steel tube by enclosing the entire resonance tube with ice. Results of endwall gas temperature with and without the ice showed that the endwall gas temperatures were affected very little by the enhanced heat conduction losses in the jet regurgitant mode.

It is believed, therefore, that the most important source of heat removal from the resonance tube, which limits the endwall gas temperature, is the periodic turbulent mixing of the cold nozzle jet flow with the oscillating hot tube flow. In the jet screech mode of operation, this turbulent mixing was minimal.

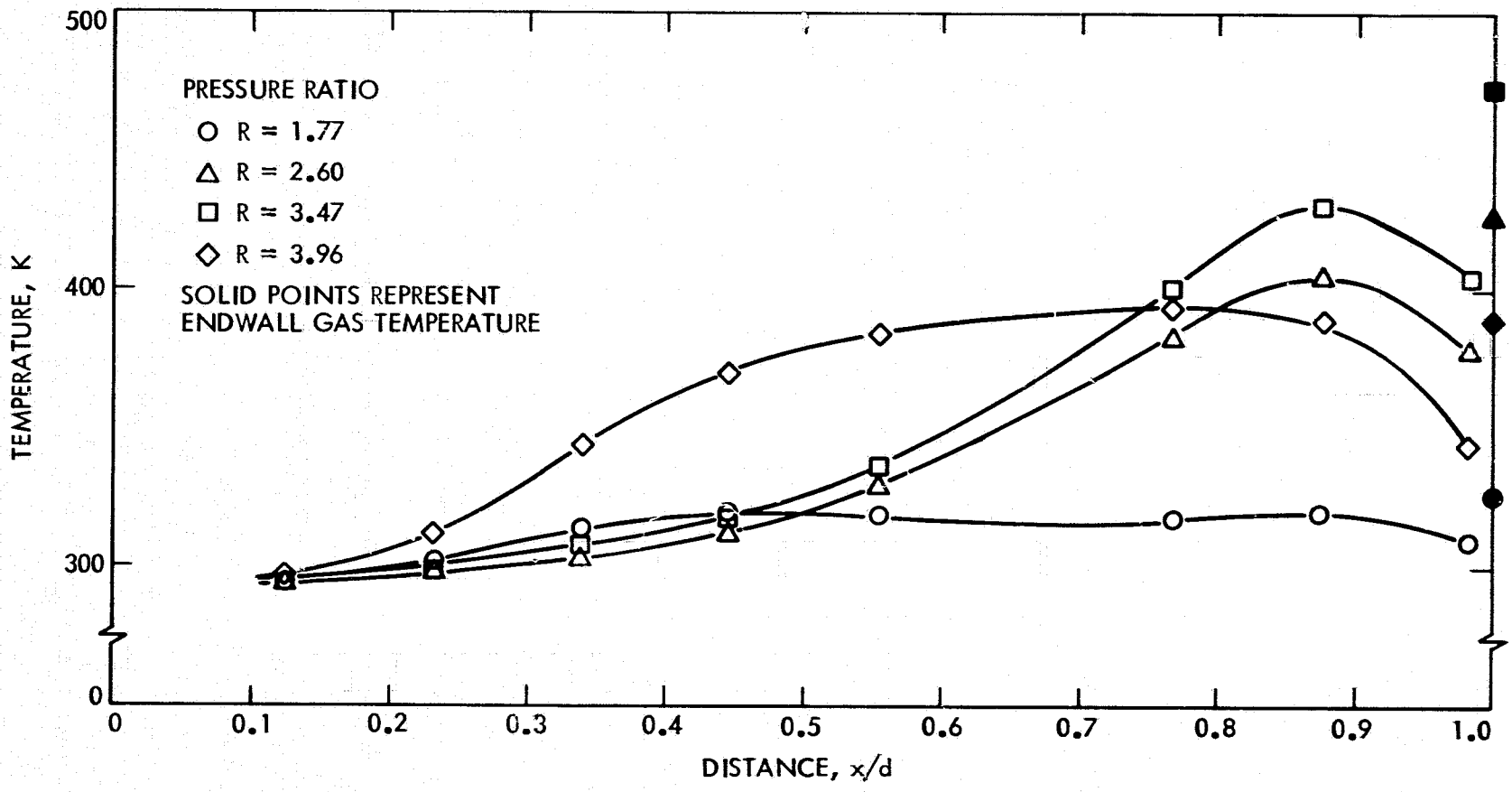

Fig. 16. Effect of nozzle pressure ratio R on wall temperature for 35.6-cm steel resonance tube with spacing s/d = 1.5

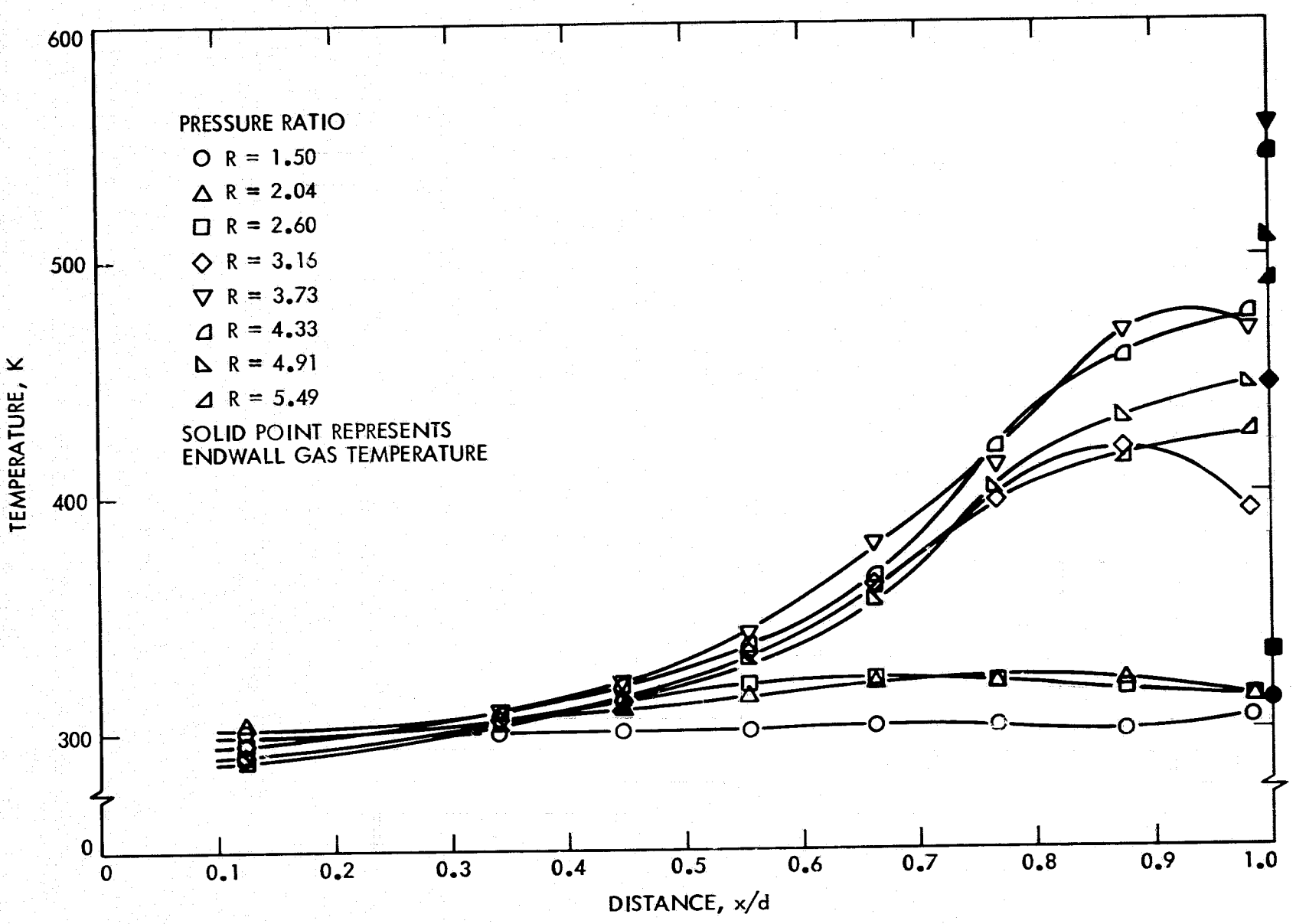

Fig. 17. Effect of nozzle pressure ratio R on wall temperature for 35.6-cm steel resonance tube with spacing s/d = 3

E. EXPERIMENTAL AND THEORETICAL WAVE SPEEDS IN RESONANCE TUBES

1. Theoretical Procedures

From theoretical considerations of simple shock wave reflection from the endwall of the tube, the following relation between the pressure jump across the incident and reflected waves can be obtained:

$$\frac{p_3 - p_2}{p_2 - p_1} = \frac{\frac{2\gamma}{\gamma + 1}\left(\frac{p_2}{p_1}\right)}{1 + \frac{\gamma - 1}{\gamma + 1}\left(\frac{p_2}{p_1}\right)} \tag{1}$$

If the pressure jumps across the incident shock wave ($p_2 - p_1$) and across the reflected shock wave ($p_3 - p_2$) are known, the pressure ratio (p_2/p_1) across the incident wave can be determined from Eq. (1). Then absolute levels of pressures p_3, p_2, and p_1 can also be determined. As discussed previously, it was not possible to measure the absolute pressure levels with the piezoelectric pressure transducers accurately because of gas heating near the endwall. The output of the quartz transducers drifted with temperature. However, from the pressure jumps across the incident and reflected shocks, which are not affected by the transducer output drift with temperature, and by use of Eq. (1), absolute levels could be determined. Also, the Mach number of the incident shock wave can then be determined from the relation

$$M_s^2 = 1 + \left(\frac{\gamma + 1}{2\gamma}\right)\left(\frac{p_2}{p_1} - 1\right) \tag{2}$$

It is then possible to evaluate all of the fluid properties behind the incident and the reflected shock waves. For example, the ratio of the contact surface velocity U_c to the incident wave velocity U_s is given by

$$\frac{U_c}{U_s} = \frac{\frac{2}{\gamma + 1}\left(\frac{p_2}{p_1} - 1\right)}{\frac{p_2}{p_1} + \frac{\gamma - 1}{\gamma + 1}} \tag{3}$$

The ratio of the reflected wave velocity to the incident shock velocity is given by

$$\frac{U_r}{U_s} = \frac{\frac{2}{\gamma + 1}\left(\frac{p_2}{p_1} - 1\right)}{\frac{p_2}{p_1} + \frac{\gamma - 1}{\gamma + 1}}\left[\frac{\frac{\gamma + 1}{2}\left(\frac{p_3}{p_2}\right) + \frac{\gamma - 1}{2}}{\left(\frac{p_3}{p_2} - 1\right)} - 1\right] \tag{4}$$

where

$$\frac{p_3}{p_2} = \frac{\left(2\,\frac{\gamma - 1}{\gamma + 1} + 1\right)\frac{p_2}{p_1} - \frac{\gamma - 1}{\gamma + 1}}{\frac{\gamma - 1}{\gamma + 1}\left(\frac{p_2}{p_1}\right) + 1} \tag{5}$$

Equations (3), (4), and (5) can be reduced to give

$$\frac{U_r}{U_s} = 1 - \left(\frac{3 - \gamma}{2}\right)\frac{U_c}{U_s} \tag{6}$$

Equation (6) is the relation among incident, contact, and reflected wave velocities, and it is apparent that the relationship depends only on the specific heat ratio of the gas. In the following section, the wave speeds measured by the laser-Schlieren technique and by the sidewall pressure transducer will be compared with the theoretical predictions given by Eq. (6).

2. Comparison of Experimental and Theoretical Results

Shock wave velocities in the jet regurgitant mode of resonance tube operation were measured using two laser beams a known distance apart. A

typical cross-correlation of the data is shown in Fig. 18. The incident, reflected, and the contact surface velocities for the 35.6-cm resonance tube with spacing s/d = 3 and pressure ratio R = 4.04 in the jet regurgitant mode are indicated in Fig. 18. In this case, the spacing between the centers of the two beams was 1.55 cm. These wave velocities were determined from the beam spacing and the delay time.

A comparison of the experimental and predicted velocities for the jet regurgitant operating mode for spacings s/d = 3 and 4 are shown in Fig. 19. The solid curve in Fig. 19 represents the theoretical prediction as given by Eq. (6). As shown in this figure, reasonably good agreement with theory was obtained.

A check on the wave velocities as obtained from the laser-Schlieren measurements was made by computing the incident, contact surface, and reflected wave velocities from the measured pressure jumps across the incident and reflected shock waves using Eqs. (1) to (6). Figure 20 shows the typical sidewall as well as the endwall pressure traces. These traces were taken for the 35.6-cm lucite tube with spacing s/d = 3 when the tube was operating in the jet regurgitant mode. The top trace in this figure was at the endwall, whereas the middle and bottom traces were at x/d = 12 and 6, respectively. The middle trace, which was close to the endwall, clearly indicates the incident and the reflected shock wave strengths. The pressure jumps across the incident and the reflected waves were read from this trace to determine the absolute levels of the pressures as well as the wave velocities inside the tube.

A typical value for the ratio of pressure jumps across the incident and across the reflected shock waves was $(p_3 - p_1)/(p_2 - p_1) = 3.53$ for the 35.6-cm resonance tube with spacing s/d = 3. This corresponds to a pressure ratio across the incident and reflected shock $p_2/p_1 \simeq 3.40$. By use of Eq. (2), the Mach number of the incident shock wave M_s was found to be 1.75. Also, the ratio of the contact surface velocity to the incident shock velocity $U_c/U_s \simeq 0.56$, and the ratio of the reflected shock wave velocity to the incident shock wave velocity $U_r/U_s \simeq 0.55$. These results are indicated on Fig. 19 and the agreement with the predicted result is reasonably good.

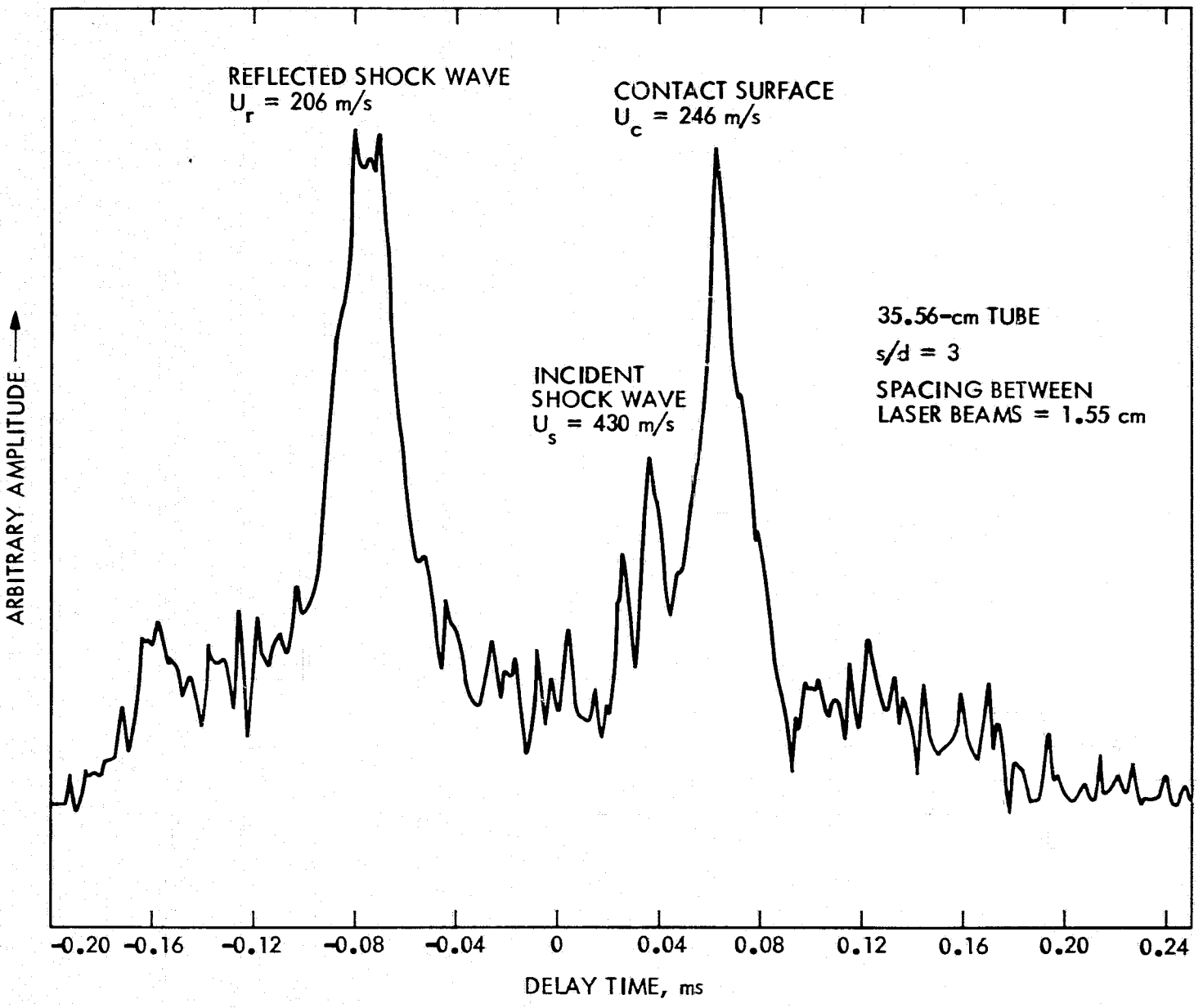

Fig. 18. Cross-correlation of laser data

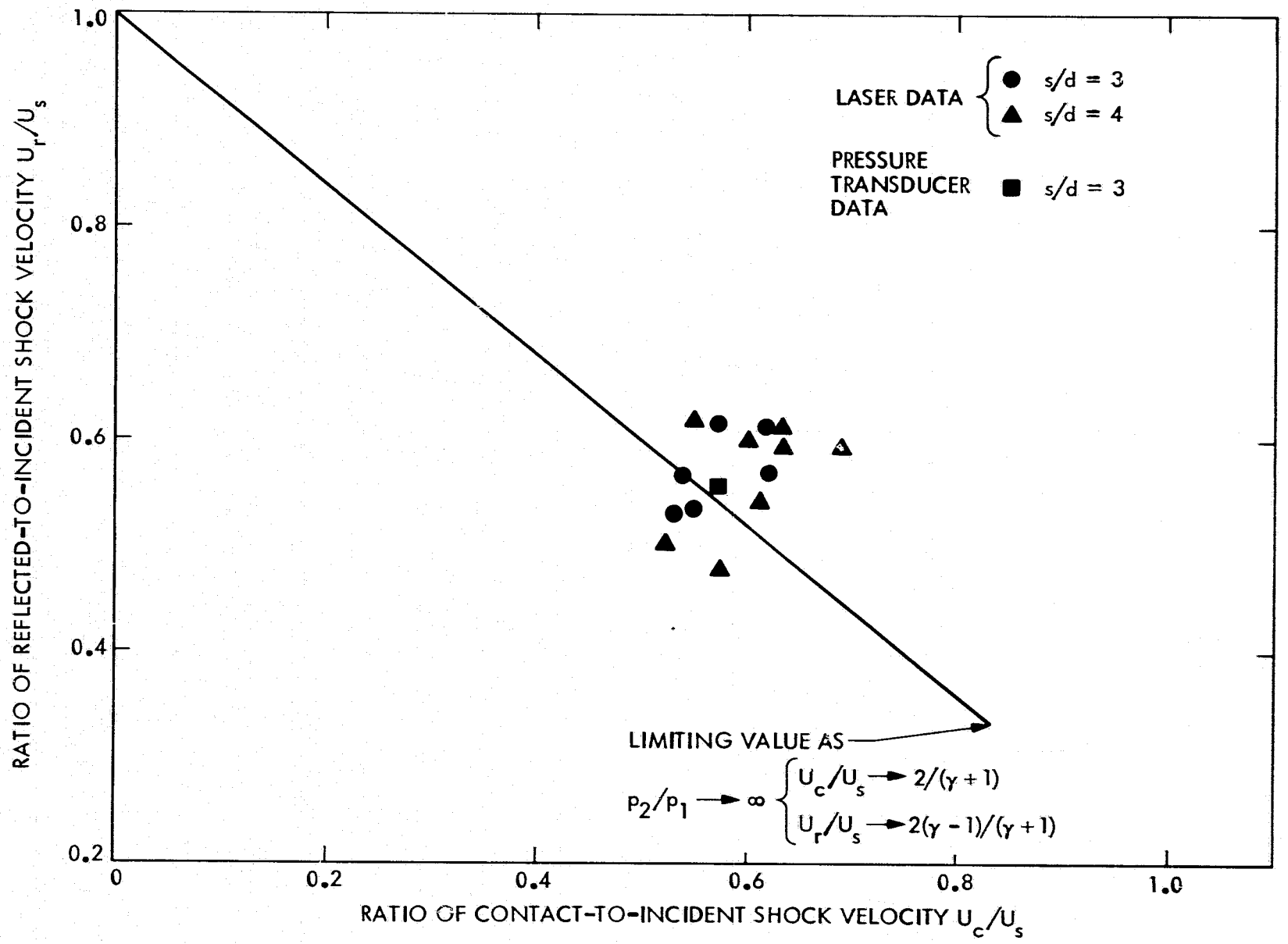

Fig. 19. Comparison of experimentally measured shock wave velocity with predicted results in regurgitant mode for 35.6-cm resonance tube operation

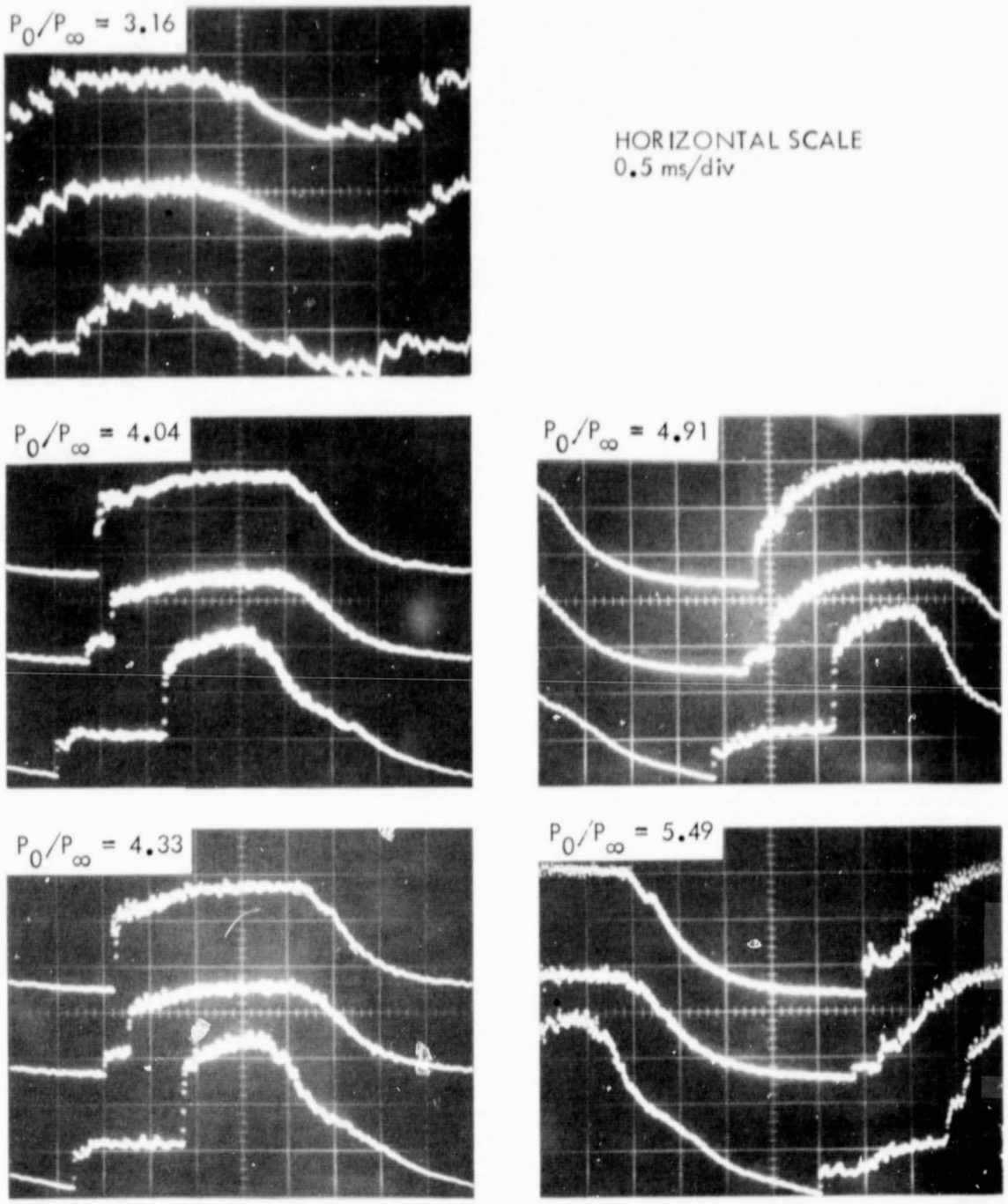

VERTICAL SCALE:

TOP TRACES (ENDWALL)	22.68 N/cm^2/div (32.89 psi/div)
MIDDLE TRACES (x/d = 12)	18.44 N/cm^2/div (26.74 psi/div)
BOTTOM TRACES (x/d = 6)	9.07 N/cm^2/div (13.16 psi/div)

Fig. 20. Typical pressure traces of 35.6-cm resonance tube at x/d = 6, x/d = 12, and endwall for different nozzle pressure ratios R with spacing s/d = 3

In the above case, the pressure jump across the incident and reflected shock wave was $p_2 - p_1 \sim 7.58$ N/cm^2 (11.0 psi) and the pressure ratio across this wave p_2/p_1 was 3.53. The absolute pressures were:

Pressure in front of the incident shock wave	$p_1 \sim 3.03$ N/cm^2 (4.4 psi)
Pressure behind the incident shock wave	$p_2 \sim 10.75$ N/cm^2 (15.6 psi)
Pressure behind the reflected shock wave	$p_3 \sim 29.78$ N/cm^2 (43.2 psi)

It should be noted that in the jet regurgitant mode, pressures below atmospheric were observed before the inflow phase was initiated. Behind the incident shock wave, the pressures were close to the atmospheric pressure of 9.86 N/cm^2 (14.3 psi).

V. CRITERIA FOR INTENSE HEATING OF RESONANCE TUBES

One of the most intriguing aspects of resonance tube performance in this investigation occurred when the tube flow switched from a regurgitant mode to a jet screech mode. To emphasize the results, the key features of this change in resonance tube mode of operation are summarized below:

(1) With increasing nozzle pressure the change of jet flow from regurgitant to screech mode resulted in drastic changes in endwall temperature as shown in Figs. 13, 14, and 15. For the 7.6-cm resonance tube there was intense heating when this change in mode occurred; however, for the 35.6-cm tube there was a drop in endwall gas temperature. On the other hand, when the pressure was increased further for the 7.6-cm resonance tube, a sudden drop in endwall gas temperature was observed.

(2) As the tube flow went into the jet screech mode, a normal shock appeared in front of the resonance tube inlet. This normal shock-wave oscillated about its mean position at high frequency. These high-frequency shock oscillations generated relatively weak waves inside the resonance tube as compared to those in the jet regurgitant mode.

(3) In comparison to the inflow phase of the jet regurgitant mode, only a small amount of nozzle jet mass flow entered the tube in the screech mode. The normal shock wave in front of the tube inlet acted like a leaky piston oscillating at a high frequency.

The cause of the intense heating in the jet screech mode over a range of nozzle pressure ratios is discussed subsequently in this section. An understanding of this mechanism can be helpful in designing a resonance tube system for a particular mode of operation.

The effect of nozzle pressure ratio on endwall gas temperature for the 7.6-cm resonance tube with spacing s/d = 2 is shown in Fig. 21. Also shown on the figure are the corresponding frequencies of the endwall pressure traces. No significant endwall gas heating occurred in the jet regurgitant mode. As the nozzle pressure was increased, in the jet regurgitant mode, the frequency of the endwall pressure trace remained almost constant at the fundamental resonance frequency of the tube, which for the 7.6-cm tube was approximately 1000 Hz. As the resonance tube switched to the jet screech mode at a nozzle pressure ratio of 5.75, the endwall pressure signal indicated a jet screech frequency of about 3500 Hz. This was accompanied by a sudden jump in the endwall gas temperature to about 900 K, accompanied by charring of the lucite tube. As the nozzle pressure ratio R was increased above 5.75, the screech frequency increased slowly until a nozzle pressure ratio of 7.85 was reached. The resonance tube flow jumped to a higher stage of jet screech with an endwall pressure signal frequency of 18 kHz. This caused a sudden drop in the endwall gas temperature.

The endwall pressure traces of the jet regurgitant, first and second stages of jet screech mode of operation for the 7.6-cm resonance tube with spacing s/d = 2, are shown in Fig. 22. The endwall pressure trace at a nozzle pressure ratio of 4.91 was at a tube resonance frequency of about 1000 Hz with the tube flow in the jet regurgitant mode. The pressure traces at nozzle pressure ratios of 5.82, 6.74, 7.28 and 7.82 were for the first stage of jet screech mode with a tube oscillation frequency of about 3500 Hz. As compared to the jet regurgitant mode, the amplitude of the waves in the tube was smaller for the first stage of jet screech mode. The intense heating in the first stage of jet screech mode was accompanied by little periodic

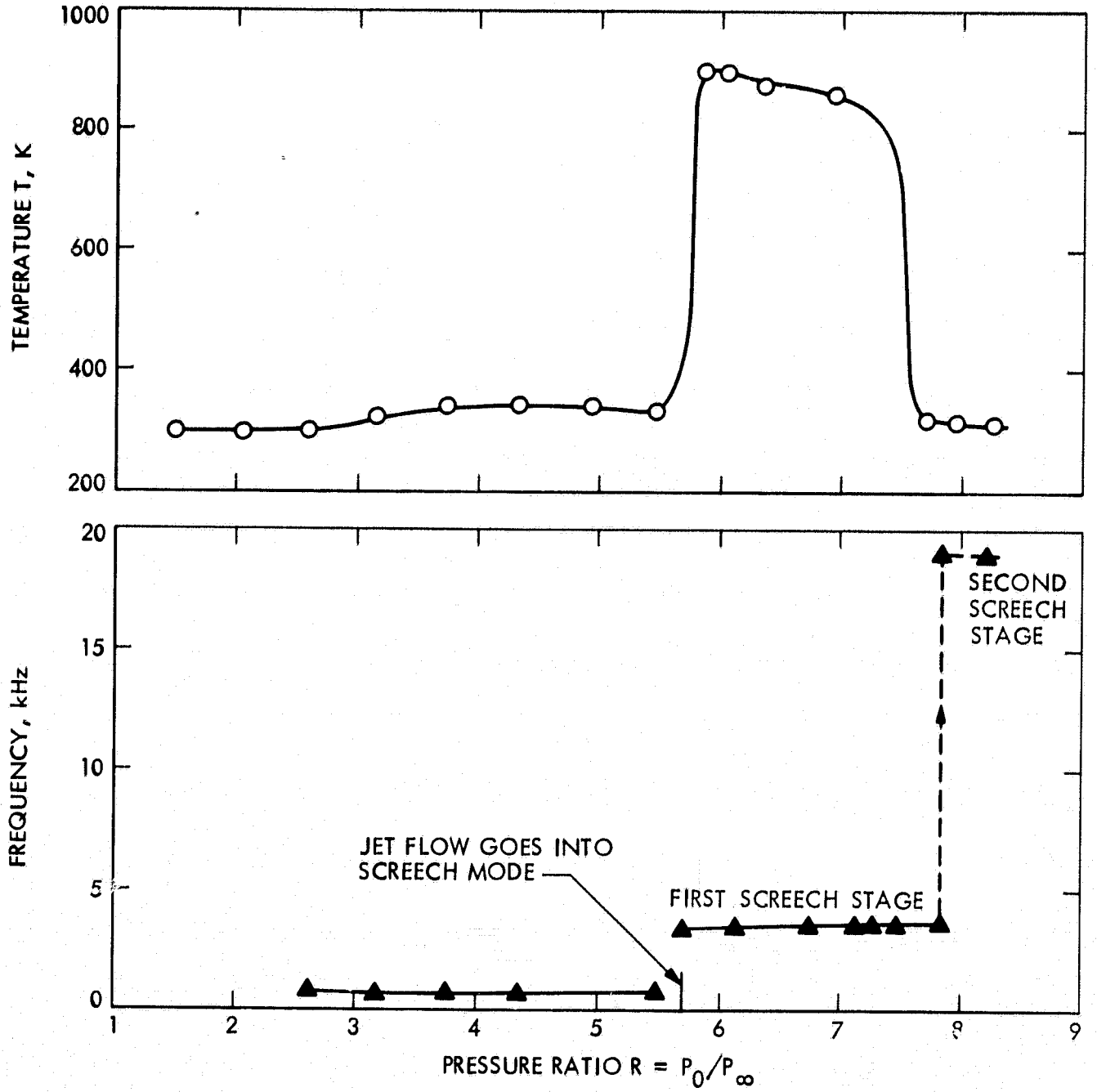

Fig. 21. Endwall gas temperature in various modes of 7.6-cm resonance tube operation with spacing s/d = 2

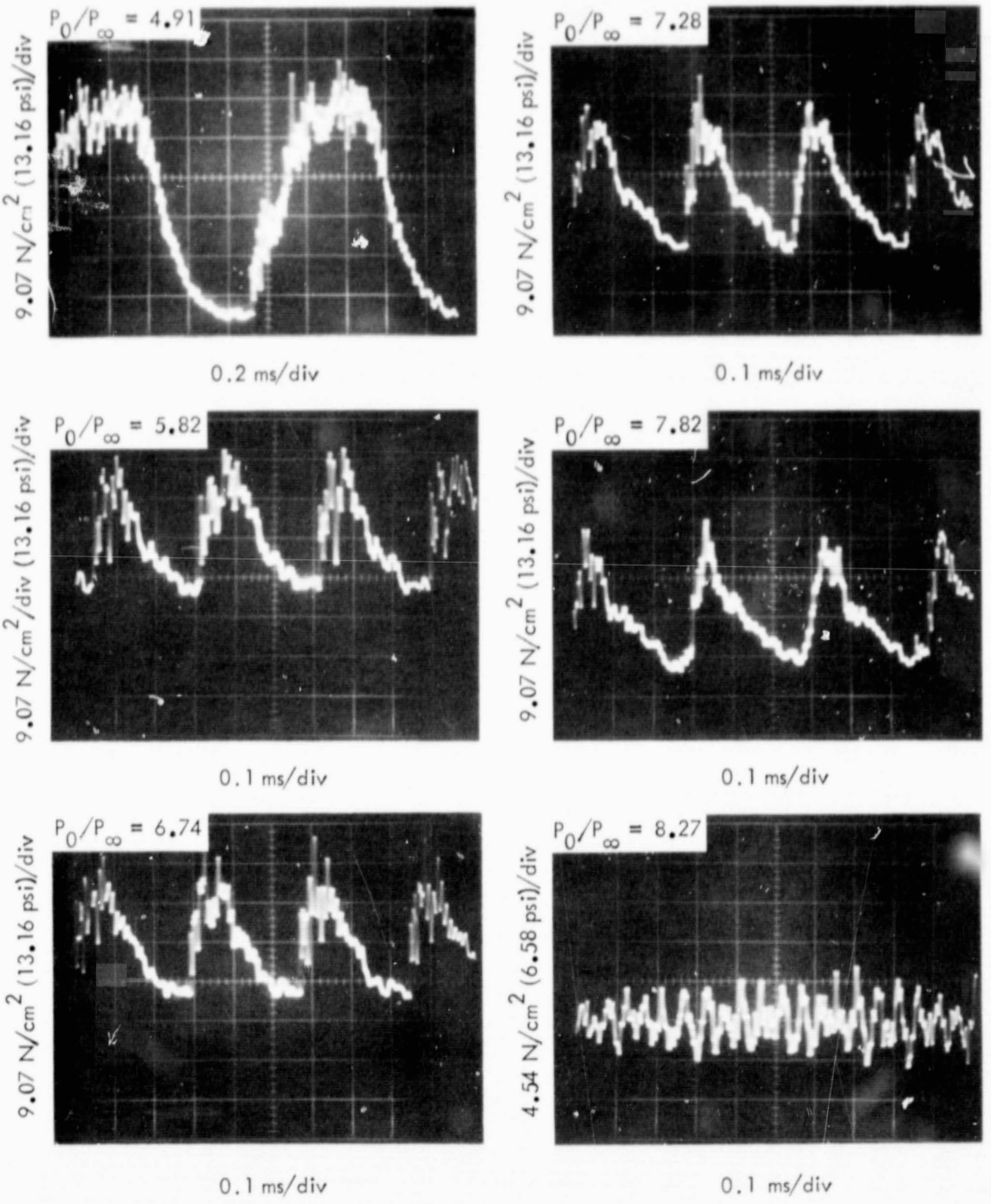

Fig. 22. Oscilioscope record of pressure at endwall of 7.6-cm resonance tube in different modes of operation with spacing s/d = 2

mass exchange between the oscillating hot tube flow and the cold nozzle jet flow. When the resonance tube flow switched to higher stages of jet screech mode at a pressure ratio of 8.27, the frequency of the waves in the tube increased to approximately 18 kHz. A pronounced reduction in endwall gas temperature was accompanied with the formation of relatively weak waves inside the tube. In comparing the amplitude of endwall pressure traces in the first and second stages of the jet screech mode in Fig. 22, it should be noted that the vertical scales are not identical.

Figure 23 indicates the jet flow in the regurgitant mode, first and second stages of screech mode. These pictures have been arranged with increasing time from top down for a typical cycle of tube operation. Set A in Fig. 23 represents the jet flow in the regurgitant mode for a nozzle pressure ratio of 4.91. Set B in Fig. 23 represents the flow in the first stage of jet screech mode during which intense heating of the endwall gas occurred. These pictures show a normal shock present constantly in front of the resonance tube. This shock wave oscillated with large amplitude in a cycle about its mean position. These large-amplitude shock oscillations subsided as the resonance tube flow switched to a higher stage of screech mode above a nozzle pressure ratio of 7.85. Typical shadowgraphs of the jet flow in the second stage of screech mode are shown in set C of Fig. 23. This jet flow configuration did not heat the endwall gas. The shadowgraphs indicated that the sudden drop in endwall gas temperature was accompanied by very-small-amplitude oscillations of the normal shock in the jet flow between the nozzle exit and the tube inlet. This resulted in comparatively weak waves inside the tube; e.g., see the pressure trace at nozzle pressure ratio of 8.27 in Fig. 22.

The amplitude of this normal shock between the nozzle exit and tube inlet in the first and in the second stages of the jet screech mode of the 7.6-cm tube with $s/d = 2$ was determined relative to the free-jet shock location $(X_s/s)_{free\text{-}jet}$ and the Mach disc $(X_m/d)_{free\text{-}jet}$ as a function of nozzle pressure ratio. The experimental results in Fig. 24 for nozzle pressures ratios less than 4.75 pertain to the regurgitant mode. The shock location in the inflow phase of the jet regurgitant mode was close to the free-jet shock location. At a nozzle pressure ratio of 5.8, when $(X_s/d)_{free\text{-}jet} \approx s/d$, the tube flow

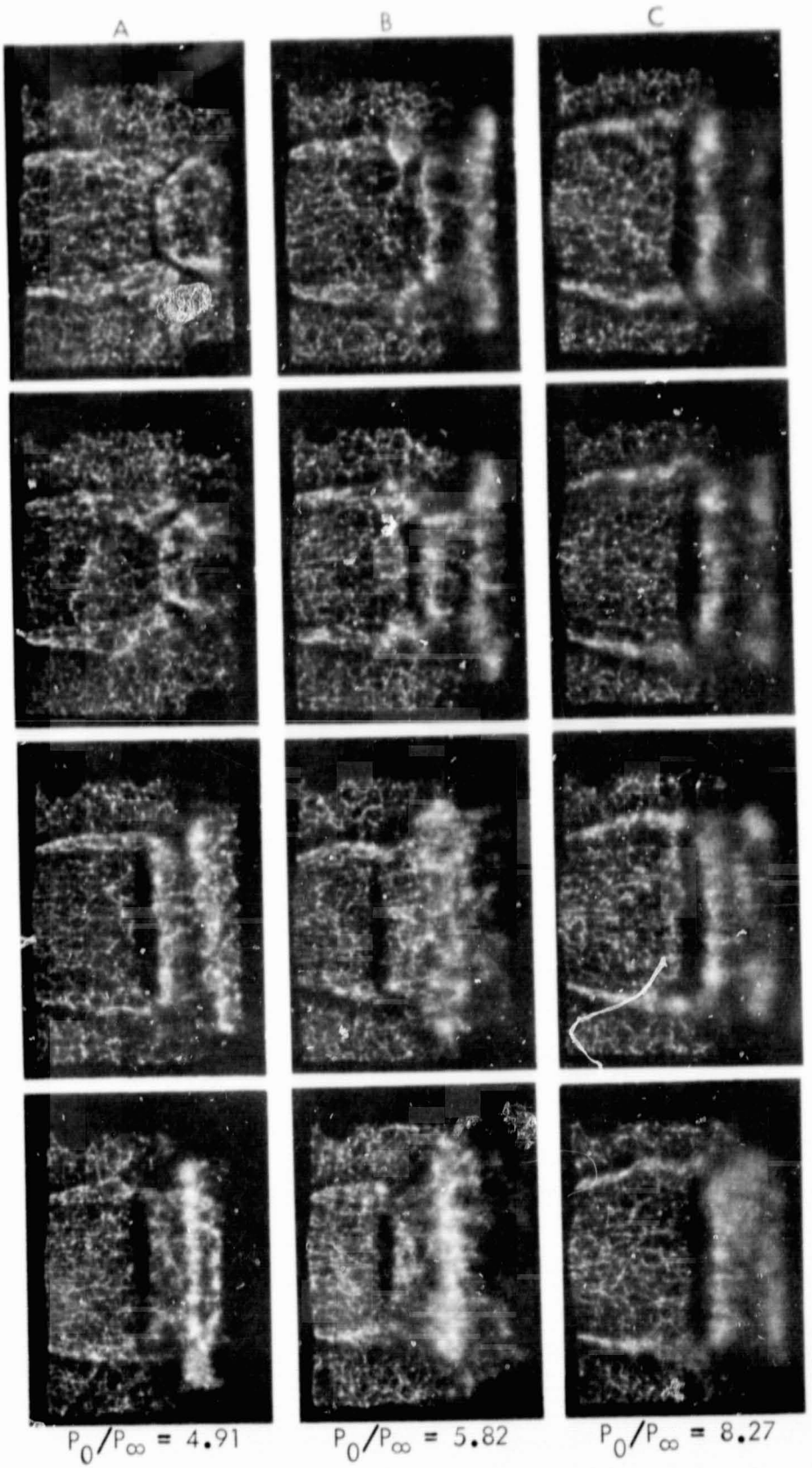

Fig. 23. Sequence of jet-flow shadowgraph pictures of 7.6-cm resonance tube in different modes of operation with spacing s/d = 2

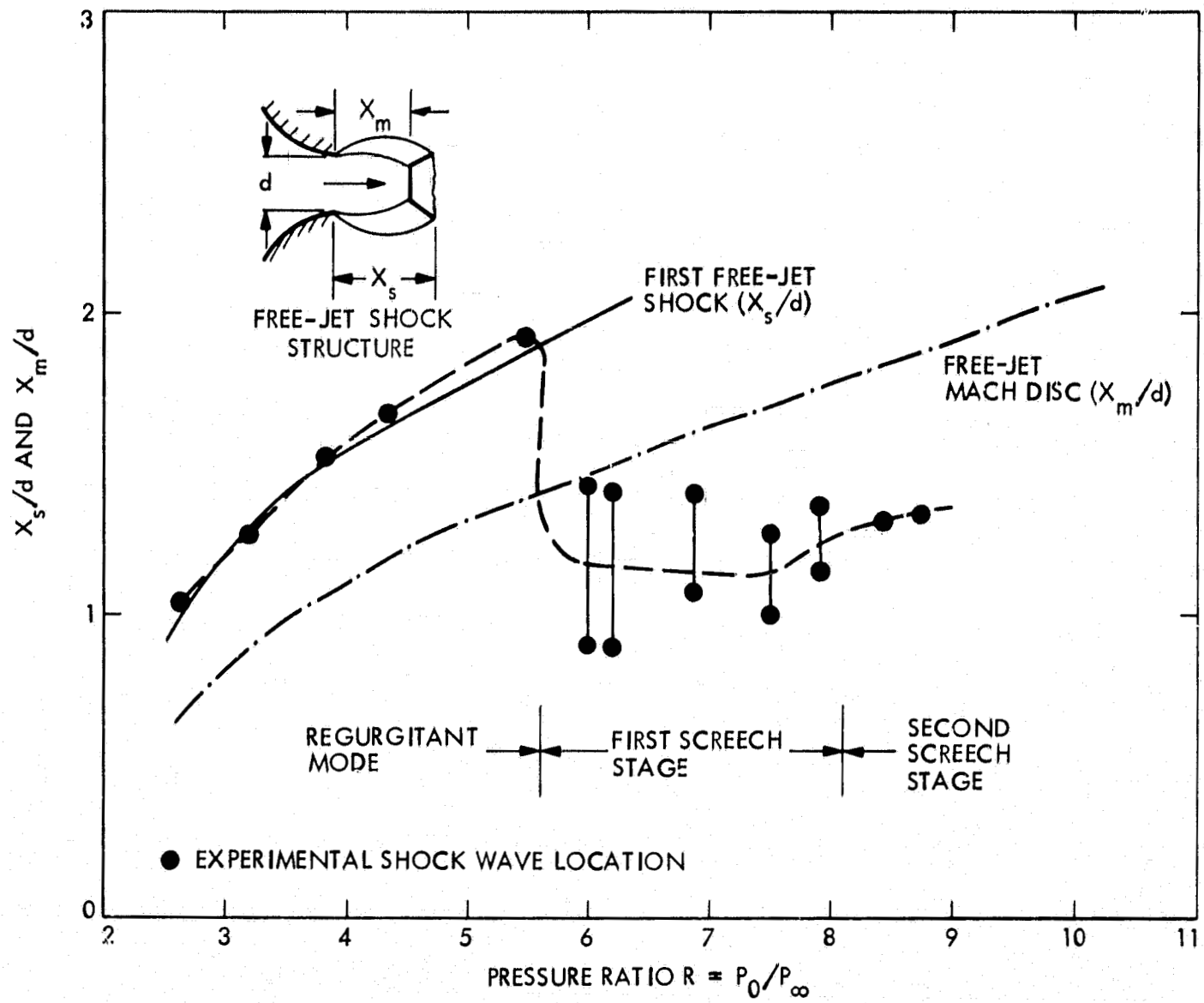

Fig. 24. Shock wave location in various modes of 7.6-cm resonance tube operation with spacing s/d = 2

switched to the first stage of jet screech mode. The large amplitude of the oscillating jet shock wave which produced an intense heating condition has been shown in Fig. 24 by joining the minimum shock location $(X_s/d)_{min}$ and the maximum shock location $(X_s/d)_{max}$ by a vertical line. This amplitude remained on the order of 10-25% of the tube spacing s/d until a nozzle pressure ratio of 7.85 was reached. The jet flow shock wave then began to oscillate at a frequency f ~ 18 kHz. The high-frequency jet flow shock oscillation had a very small amplitude and did not cause any heating of the endwall gas temperature.

The intense heating of the endwall gas in the first stage of screech mode resulted in charring of the lucite tube. Two such charred tubes, 7.6 and 17.8 cm in length, are shown in Fig. 25. On critical analysis of these tubes it was concluded that large-amplitude oscillations of the shock wave in the jet flow were accompanied by standing waves inside the tube. As shown clearly in Fig. 25, locally heated node points indicate the presence of standing waves inside the tube.

On the basis of the above results, it is asserted that maximum heating of the endwall gas occurred in the jet screech mode. To obtain this intense heating, it is believed that the jet flow shock oscillation frequency should be in tune with one of the resonance frequencies of the tube; i.e.,

$$f_{shock} = f_{tube} \equiv \frac{a}{L}\left(\frac{2N+1}{4}\right)$$

where N can take values 0, 1, 2, 3 • • • • depending upon various resonance frequencies of the tube. This intense heating is characterized as follows:

(1) Large-amplitude oscillations of the normal shock between the nozzle exit and the tube inlet occur.

(2) As compared to the inflow phase of the jet regurgitant mode, a small fraction of the nozzle jet flow enters the tube. Consequently, little mass exchange results during each cycle of the jet screech mode.

(3) Most of the dissipative heat energy generated by irreversible processes across the compression wave fronts is trapped between the node points of the tuned intense heating resonance tube system in the jet screech mode. Because of reduced mass

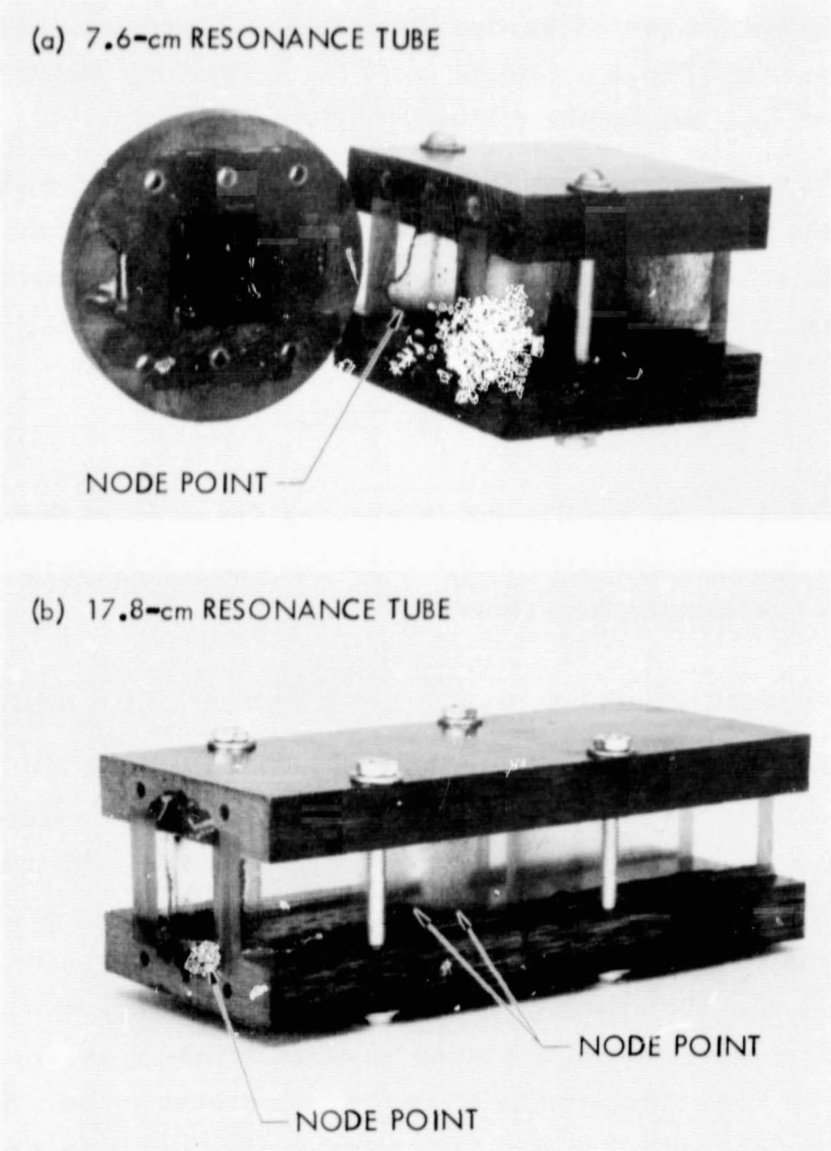

Fig. 25. Resonance tubes showing burned areas near node points caused by standing waves inside tube

exchange between the cold nozzle jet flow and the oscillating hot tube flow in each jet screech mode cycle (which is believed to be the principal source of heat removal from resonance tubes), intense heating of the gas near the endwall results. This is due to cumulative heat addition to the trapped endwall gas by dissipative processes across these high-frequency compression waves. These originate from the screeching shock wave in the jet flow acting like a "leaky" driving piston.

(4) As the resonance tube flows go out of resonance with the oscillating shock wave, e.g., with a higher stages of jet screech mode such as shown in Fig. 21, no standing waves appear inside the tube and insignificant heating of the endwall gas occurs.

VI. DISCUSSION

A summary of the results and inferences drawn from them are discussed here together with a discussion of the need for additional investigation of the phenomenon of resonance tube flows.

A. FLUID DYNAMICS OF VARIOUS RESONANCE TUBE MODES

According to Hartmann (Ref. 2), high intensity sound vibrations are generated when the resonance tube is placed in the region where the pressure in the jet is rising, i.e., the spatial zone of instability. The present measurements show that the regurgitant and screech modes are separated when this zone of spatial instability for free-jet begins, i.e., free jet shock location X_s, is equal to the spacing s, for a given jet flow condition. The results in Fig. 4 can be used to design a given resonance tube system to operate either in the jet regurgitant mode or in the jet screech mode. Results of the present experiments indicate that the criterion for operating a given resonance tube system in the jet screech mode (i.e., to have the corresponding free-jet shock location $X_s/d_{free\text{-}jet}$ greater than the spacing s/d) works well until the shear layer behind the Mach disc begins to interact with the resonance tube inlet. It is believed that the tube inlet configuration also plays a role when a switch from regurgitant to screech mode occurs, e.g., the ratio of

free-jet Mach disc diameter to tube inlet diameter. This interaction of the shear layer between the oscillating shock wave and resonance tube inlet at higher nozzle pressure ratios may have resulted in the departure of the experiments from the above criterion in separating the regions of jet regurgitant and screech modes (Fig. 4). Further experiments investigating the influence of the tube inlet configuration on various resonance tube modes are needed. This investigation will assist in designing a given tube system to operate in a particular mode.

In the jet screech mode, the shock wave in the jet flow oscillated in various bands of frequencies, as has previously been observed (Refs. 2 and 7). In each band of jet flow screech operation, the oscillation frequency of the shock wave decreased with an increase of spacing for a given nozzle pressure and increased with increasing nozzle pressure with a fixed spacing s/d (Refs. 2 and 7). This behavior of the jet flow shock wave oscillation in the jet screech mode indicates that these oscillations may be driven by the shear layer located behind this shock and the resonance tube inlet. Such shear flows are inherently unstable and are known to sustain periodic oscillations (Refs. 17 and 18). Additional studies of this shear flow between the oscillating shock and the resonance tube inlet in the jet screech mode would shed more light on these self-sustained oscillations of the shock wave.

B. HEATING OF THE RESONANCE TUBE GAS

Shadowgraphs in the inflow phase of the jet regurgitant mode showed that most of the jet flow entered the tube. This resulted in formation of an almost normal shock, followed by a contact surface. This contact surface separated the oscillating hot tube gas from the entering nozzle jet flow. Shadowgraphs showed a strong mixing and large-scale turbulent motion when the contact surface collided with the reflected shock wave. It is believed that the contact surface due to rushing nozzle jet flow (during the inflow phase of the jet regurgitant mode) may not be plane wave. Owing to nonuniform contact surface waves, large periodic turbulent mixing may result between the nozzle-jet cold gas and the oscillating hot gas inside the resonance tube (Figs. 7H and J). Therefore, most of the heat generated in the jet regurgitant mode, which occurs mainly by dissipative processes across the shock waves and is formed in the tube in the inflow phase of the regurgitant mode

cycle, is carried away periodically by the tube jet flow during the outflow phase of the regurgitant mode. This source of heat removal in the jet regurgitant mode has not been taken into account in the theoretical procedures of Shapiro (Ref. 14) and of Wilson and Resler (Ref. 13). This may be the main reason why the predicted temperatures of the tube gas are much higher than the measured ones in the jet regurgitant mode of resonance tube operation.

VII. CONCLUSIONS

From this investigation, the following conclusions have been drawn:

(1) Of the three modes of resonance tube operation, maximum heating of the tube gas occurs in the screech mode when the tube is in resonance with the jet-flow shock-wave oscillation frequency. The highest endwall gas temperature was about 900 K before tube failure occurred.

(2) Various modes of resonance tube operation are independent of the length of the tube. They critically depend upon the nozzle pressure ratio, spacing between the nozzle exit and tube inlet, the shape of the tube inlet, etc.

(3) Screech mode of resonance tube operation occurred within Hartmann's "region of instability," in which the jet flow shock oscillates in various frequency bands. Drastic changes in endwall gas temperature occur when the jet flow shock-wave oscillation frequency changes among various screech modes.

(4) Substantial turbulent mixing of the cold nozzle jet flow and the oscillating hot tube flow results during the inflow phase of the jet regurgitant mode. In the outflow phase of the jet regurgitant mode, the tube jet removes this heat from the resonance tube. This periodic mass efflux from the tube is the main source which limits the rise of the temperature of the gas in the vicinity of its endwall. In the jet screech mode, however, not much nozzle jet flow entered the tube. Therefore, the turbulent mixing of the cold nozzle jet flow and the oscillating tube flow was minimal. If the length of the tube is such that the tube is tuned to the

jet flow shock oscillation frequency, intense and rapid heating of the tube gas between the node points results.

(5) In the jet regurgitant mode of resonance tube operation, pressures below atmospheric were observed before the beginning of the inflow phase. Behind the incident shock wave, pressures close to ambient pressure were observed, as proposed by Brocher et al. (Ref. 1).

(6) Very little heating of the gas inside the tube occurs in the event that there are leaks in the vicinity of the tube endwall or through the interface between the sidewalls.

DEFINITIONS OF TERMS

a	average speed of sound in the resonance tube
D	steel resonance tube diameter or width of the square cross-sectional resonance tube
d	exit diameter of nozzle
f	frequency, Hz
L	resonance tube length
$M_s = \frac{U_s}{a}$	incident shock wave Mach number
p	static gas pressure
P_0	nozzle stagnation pressure
P_∞	ambient pressure
$R = \frac{P_0}{P_\infty}$	nozzle pressure ratio
s	spacing between nozzle exit and tube inlet
t	time
T	temperature, K
U_c	velocity of contact surface
U_j	mean velocity in x direction at nozzle exit
U_r	velocity of reflected shock wave
U_s	velocity of incident shock wave
x	streamwise coordinate along the resonance tube
X_s	location of free-jet shock wave from nozzle exit (see Fig. 24)
X_m	location of free-jet Mach disk from nozzle exit (see Fig. 24)
γ	specific heat ratio

$(\ )_{\text{free-jet}}$	corresponds to conditions without the presence of resonance tubes in jet flows
$(p)_{1,2,3}$	corresponds to static pressure in front of incident shock, behind incident shock, and behind reflected shock waves, respectively.

REFERENCES

1. Brocher, E., Maresca, C., and Bournay, M. H., "Fluid Dynamics of the Resonance Tube," J. Fluid Mech., Vol. 43, Part 2, pp. 369-384, 1970.

2. Hartmann, J., "On the Production of Acoustic Waves by Means of an Air-Jet of a Velocity Exceeding that of Sound," Phil. Mag., Vol. 11, No. 72, pp. 926-948, Apr. 1931.

3. Stabinsky, Leon, Analytical and Experimental Study of Resonance Ignition Tubes, Rocketdyne Division, Rockwell International Report 9403, Dec. 1973.

4. Marchese, P. Vincent, Development and Demonstration of Flueric Sounding Rocket Motor Ignition, NASA-CR-2418, June 1974.

5. Morris, Joseph W., "Flueric Cartridge Initiator Development," Naval Ordnance Station, Indian Head, Maryland, paper presented at the Los Alamos Scientific Laboratory, Los Alamos, New Mexico, Oct. 7-9, 1975.

6. Rozenberg, L. D. (editor), Source of High-Intensity Ultrasound, Translated from Russian, Plenum Press, New York, 1969.

7. Brun, E., and Boucher, R. M. G., "Research on the Acoustic Air-Jet-Generator. A New Development," J. Acoust. Soc. Am., 29 (5), May 1957.

8. Sprenger, H. S., "Uber Thermische Effckte bei Rezonanzrohrem," Mitteilungen aus dem Institut für Aerodynamik an der E. T. H., Zurich, Nr. 21, pp. 18-35, 1954 (AERE lib/trans. 687).

9. Thompson, Philip A., "Resonance Tubes," Ph.D. Thesis, Massachusetts Institute of Technology, Dec. 1960.

10. Brocher, E., and Maresca, C., "Etude des Phenomenes Thermignes dans un Tube de Hartmann-Spreuger," Int. J. Heat Mass Transfer, Vol. 16, Pergamon Press, pp. 529-548, 1973 (NASA Technical Translation F-14, 796).

11. Vrebalovich, T., Resonance Tubes in a Supersonic Flow Field, Technical Report No. 32-378, Jet Propulsion Laboratory, Pasadena, Calif., July 1962.

12. Lloyd, E. C., Pressure Wave Propagation in a Resonance Tube, National Bureau of Standards Report 6443, June 1958.

13. Wilson, J., and Resler, E. J., Jr., "A Mechanism of Resonance Tubes," J. Aerosp. Sc., Vol. 26, No. 7, pp. 461-462, July 1959.

14. Shapiro, Ascher, H., "On the Maximum Attainable Temperature in Resonance Tubes," J. Aerosp. Sci., Vol. 27, No. 1, pp. 66-67, Jan. 1960.

15. Mørch, K. A., "A Theory for the Mode of Operation of the Hartmann Air Jet Generator," J. Fluid Mech., Vol. 20, Part 1, pp. 141-159, 1964.

16. Westley, R., and Woolley, J. H., "An Investigation of the Near Noise Field of a Chocked Axi-symmetric Air-Jet," Proceedings of the AFOSR-UTIAS Symposium on Aerodynamic Noise, held at Toronto, Canada, May 20-21, 1968.

17. Sarohia, V., "Experimental Investigation of Oscillations in Flows Over Shallow Cavities," AIAA Paper No. 76-182, 14th Aerospace Sciences Meeting, Washington, D. C., Jan. 26-28, 1976.

18. Karamcheti, K., and Bauer, A. B., "Edgetone Generation," Stanford University, Dept. of Aero. and Astro., Report SUDAER 162, July 1963.

NASA—JPL—Coml., L.A., Calif.